Seasonal and interannual variability of the mineral dust cycle under present and glacial climate conditions

M. Werner,[1,2] I. Tegen,[1] S. P. Harrison,[1] K. E. Kohfeld,[1] I. C. Prentice,[1] Y. Balkanski,[3] H. Rodhe,[4] and C. Roelandt[1,5]

Received 23 March 2002; revised 17 July 2002; accepted 17 July 2002; published 18 December 2002.

[1] We present simulations of the dust cycle during present and glacial climate states, using a model, which explicitly simulates the control of dust emissions as a function of seasonal and interannual changes in vegetation cover. The model produces lower absolute amounts of dust emissions and deposition than previous simulations of the Last Glacial Maximum (LGM) dust cycle. However, the simulated 2- to 3-fold increase in emissions and deposition at the LGM compared to today, is in agreement with marine- and ice-core observations, and consistent with previous simulations. The mean changes are accompanied by a prolongation of the length of the season of dust emissions in most source regions. The increase is most pronounced in Asia, where LGM dust emissions are high throughout the winter, spring and summer rather than occurring primarily in spring as they do today. Changes in the seasonality of dust emissions, and hence atmospheric loading, interact with changes in the seasonality of precipitation, and hence of the relative importance of wet and dry deposition processes at high northern latitudes. As a result, simulated dust deposition rates in the high northern latitudes show high interannual variability. Our results suggest that the high dust concentration variability shown by the Greenland ice core records during the LGM is a consequence of changes in atmospheric circulation and precipitation locally rather than a result of changes in the variability of dust emissions. *INDEX TERMS:* 0305 Atmospheric Composition and Structure: Aerosols and particles (0345, 4801); 0315 Atmospheric Composition and Structure: Biosphere/atmosphere interactions; 1615 Global Change: Biogeochemical processes (4805); 3319 Meteorology and Atmospheric Dynamics: General circulation; 3344 Meteorology and Atmospheric Dynamics: Paleoclimatology; *KEYWORDS:* dust, mineral aerosol, glacial climate, GCM simulation, LGM, GRIP/GISP ice cores

Citation: Werner, M., I. Tegen, S. P. Harrison, K. E. Kohfeld, I. C. Prentice, Y. Balkanski, H. Rodhe, and C. Roelandt, Seasonal and interannual variability of the mineral dust cycle under present and glacial climate conditions, *J. Geophys. Res.*, *107*(D24), 4744, doi:10.1029/2002JD002365, 2002.

1. Introduction

[2] Marine, terrestrial and ice-core records indicate that the Last Glacial Maximum (LGM, approximately 21,000 calendar years B.P.) was characterized by a more active dust cycle, with rates of mineral dust deposition approximately 2–5 times greater than today in the tropics and midlatitudes, and up to 20 times greater than today in polar regions [see *Kohfeld and Harrison*, 2001, and references therein]. Initial attempts to simulate these changes as a direct consequence of the glacial climate, and in particular increased wind speeds, reduced strength of the hydrological cycle and changes in dust transport pathways brought about by atmospheric circulation changes, could account for only a small part of the observed strengthening of the dust cycle at the LGM [see, e.g., *Joussaume*, 1990; *Genthon and Armengaud*, 1995]. More recent simulations have reproduced both the overall magnitude and the large-scale spatial patterns of the LGM dust cycle by taking into account long-term (centennial to millennial scale) changes in dust source areas as a consequence of climatically induced changes in soil hydrology [e.g., *Andersen et al.*, 1998] and vegetation [e.g., *Mahowald et al.*, 1999]. Indeed, *Mahowald et al.* [1999] suggested that these changes in dust source areas were the dominant cause of the strengthening of the dust cycle at the LGM.

[3] The modern dust cycle is characterized by high short-term (interannual to interdecadal) variability in both emissions [e.g., *Middleton and Goudie*, 2001] and deposition [*Pye and Zhou*, 1989]. High-resolution ice-core records from both Greenland and Antarctic [*Steffensen*, 1988; *Taylor et al.*, 1993; *Hansson*, 1994; *Ram and Koenig*, 1997; *Ram et al.*, 1997; *Fuhrer et al.*, 1999] suggest that the increased average dust concentration in ice cores at the

[1]Max-Planck-Institute for Biogeochemistry, Jena, Germany.
[2]Formerly at Department of Meteorology, Stockholm University, Stockholm, Sweden.
[3]Laboratoire des Sciences du Climat et de l'Environnement, U.M.R. CEA-CNRS, Gif-sur-Yvette, France.
[4]Department of Meteorology, Stockholm University, Stockholm, Sweden.
[5]Now at Department of Geography, Université Catholique de Louvain, Louvain-la-Neuve, Belgium.

0148-0227/03/2002JD002365$09.00

LGM was associated with short-term variability in dust deposition significantly greater than today. The causes of this increased variability are unknown. Short-term changes in vegetation cover (which would impact on dust emissions) and short-term variations in the polar circulation (which would change the balance between wet and dry deposition) have been invoked as possible explanations [*Mayewski et al.*, 1994; *Alley et al.*, 1995; *Mayewski et al.*, 1997].

[4] In principle, the causes of changes in the variability of dust deposition in polar regions can be addressed using a model of the dust cycle. For this purpose, dust sources need to be determined as a function of the seasonal cycle of vegetation cover, snow cover and soil hydrology, and the dust source scheme must explicitly incorporate the dependence of emissions on vegetation phenology. Recent work by *Tegen et al.* [2002] has shown that a realistic simulation of the seasonality of modern dust emissions can be achieved by taking into account the existence of geomorphically favorable sites for dust sources (a point also demonstrated by *Ginoux et al.* [2001]) and by prescribing the seasonal cycle of vegetation in semi-arid regions based on satellite data. Tegen et al.'s simulation is among the first to produce, for example, both a realistic spring peak in dust emissions from Asia and a summer maximum of emissions from northern Africa. Summer atmospheric dust concentrations in the western North Atlantic region are up to an order of magnitude lower than observations, while the model results agree relatively well with observations at remote North Pacific locations downwind of the Asian continent (see also discussion by *Tegen et al.* [2002]).

[5] In this paper, we extend the model developed by *Tegen et al.* [2002] to include a prognostic simulation of vegetation phenology, allowing us to simulate the seasonal cycle of vegetation coverage and dust emissions in a changed climate. We use this model to simulate the modern and LGM dust cycles, including their seasonal and interannual variability. Analyses of these simulations enable us to address the question of the relative roles of temporal changes in emission, transport and deposition patterns in explaining observed changes in the variability of dust deposition bxoth in polar regions and elsewhere.

2. Dust Cycle Model and Analytical Approach

2.1. Modeling Strategy

[6] The dust cycle model consists of a scheme to predict dust sources, an emission scheme, a tracer transport model, and a deposition scheme. The dust cycle model is driven by climate data (wind fields, temperature, precipitation, net radiation) derived from an atmospheric general circulation model (AGCM) simulation of the present and Last Glacial Maximum (LGM, approximately 21,000 yr B.P.) climate. Since the dust model is run "offline" from the climate model, the simulations do not take into account feedbacks between the simulated atmospheric dust loading and the climate.

[7] Model performance under modern conditions is evaluated using observations from the Dust Indicator and Records of Terrestrial and Marine Palaeoenvironments (DIRTMAP) database [*Kohfeld and Harrison*, 2001]. The current version of this database contains over 300 dust records from various terrestrial, marine and ice core archives. Here we limit our comparison to dust accumulation records calculated from mass estimates from polar ice cores, modern marine sediment traps and terrigenous accumulation in marine sediments. We specifically exclude terrestrial dust records, which might be strongly influenced by local, small-scale dust sources and deposition processes not well reproduced at the coarse scale of our dust model.

[8] In order to assess how well our prognostic model of vegetation performs, we compare the simulated seasonal cycle of vegetation directly with satellite-derived reconstructions of seasonal changes in vegetation cover [*Braswell et al.*, 1997]. We also compare our modern dust cycle simulations with the results from the *Tegen et al.* [2002] simulations, which were derived using satellite-derived prescribed seasonal changes in vegetation cover and climate data from the European Center for Medium-Range Weather Forecast (ECMWF) reanalysis. The simulated mean changes in the dust cycle between the LGM and the present are evaluated using dust records derived from ice-core and marine sediment-core data archived in the DIRTMAP database [*Kohfeld and Harrison*, 2001].

[9] Although it should be possible to derive records of interannual variability in dust deposition fluxes at the LGM from annually-laminated lake sediments [e.g., *Hu et al.*, 1999; *Zolitschka et al.*, 2000], the only records of multi-annual variability that are currently available are from ice core records from the polar regions [*Steffensen*, 1988; *Taylor et al.*, 1993; *Hansson*, 1994; *Ram and Koenig*, 1997; *Ram et al.*, 1997; *Fuhrer et al.*, 1999]. We therefore compare the interannual variability of our simulations with these records.

2.2. Dust Cycle Model

[10] The offline dust cycle model includes the prediction of dust sources, an emission scheme, dust transport in the atmosphere, and a deposition scheme (Figure 1). In the dust source scheme, the extent of geomorphic situations that are favorable to dust deflation (specifically former lake beds) is explicitly determined using a high-resolution water-routing model (HYDRA [*Coe*, 1998]) and the texture of the superficial deposits within these so-called "preferential dust source regions" is specified to be predominantly silt sized [*Tegen et al.*, 2002]. Active dust sources, both in "preferential dust source regions" and elsewhere, are then determined as a consequence of vegetation type and phenology, snow cover, and soil hydrology.

[11] The dust source scheme initially simulates the equilibrium distribution of 28 major vegetation types (biomes) as a function of climate, atmospheric CO_2 concentration and soil properties (maximum soil-water holding capacity) using the BIOME4 coupled biogeography and biogeochemistry model [*Kaplan*, 2001]. Biomes arise from combinations of 13 plant functional types (PFTs) with distinct physiological, phenological and bioclimatic characteristics. BIOME4 implicitly simulates competition between these PFTs as a function of relative net primary productivity (NPP) and uses an optimization algorithm to calculate the maximum sustainable leaf area (LAI) of each PFT, and the associated NPP. In the current version of BIOME4, the spatial variation in maximum soil-water holding capacity is specified from a data set derived from the Food and Agriculture Organization (FAO) global soils map [*FAO*, 1995; *Kaplan*, 2001] and the

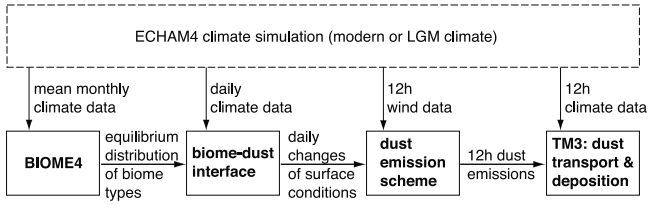

Figure 1. Schematic overview of the dust cycle model and its different components.

model is forced with monthly mean values of temperature, precipitation and net radiation interpolated to the daily time step used by the model to calculate soil hydrology.

[12] The daily evolution of vegetation cover within each biome is simulated using a biome-dust interface algorithm. This algorithm requires the same inputs (temperature, precipitation and net radiation, atmospheric CO_2 concentration, maximum soil-water holding capacity) as the BIOME4 model. The algorithm assumes that the mean fraction of absorbed photosynthetically active radiation (FPAR) can be used as a surrogate for the fraction of each grid cell covered by vegetation. FPAR is determined from the simulated leaf area index (LAI) of each PFT present using the relationship: $FPAR = 1 - \exp(-0.5/LAI)$ [*Monsi and Saeki*, 1953]. The mean value of FPAR is a proportional average of the simulated FPAR for each PFT present. The presence/absence and relative importance of each PFT is specified from the BIOME4 simulations. Evergreen PFTs are assumed to have a constant LAI throughout the year. In deciduous PFTs, the evolution of LAI during the growing season is determined by several factors. The timing of initial leaf-out is determined by a combination of the accumulated temperature sum, air temperature, soil moisture conditions and day length. Both the accumulated temperature sum and the day length required to trigger growth are PFT-specific. Plants do not respond to instantaneous drought stress, and so the soil moisture criterion for growth initiation is estimated based on a running average over 3 days and that for death due to drought stress on a running average over 5 days. In addition to drought stress, leaf death is triggered by the reduction in day length below a threshold value. Simulated daily LAI also decreases (and eventually becomes zero) as the leaves become old. The maximum leaf longevity is PFT specific.

[13] To derive the effective surface fraction A_{eff} for dust emission in each grid cell from the vegetation cover surrogate FPAR, we apply the same approach as *Tegen et al.* [2002]. For grass-dominated biomes we assume that dust deflation can occur whenever the green vegetation is below a certain limit ($FPAR < 0.25$). This limit prevents dust emissions by modest and dense grass cover. The effective dust source area A_{eff} increases linearly with decreasing vegetation to a maximum of $A_{eff} = 1$ for $FPAR = 0$:

$$\text{for grass} - \text{dominated biomes}: \quad A_{eff} = \begin{cases} 1 - FPAR & \text{if } FPAR \le 0.25 \\ 0 & \text{otherwise} \end{cases}.$$

[14] For shrub-dominated biomes we must use a different calculation of A_{eff} since shrubs can protect the soil surface even when no leaves are present ($FPAR = 0$). For shrub-dominated tundra biomes we assume that the effective vegetation cover is constant throughout the year and equals the annual maximum of FPAR. Again, we set a limit of $FPAR(max_{ann}) < 0.25$ to prevent dust emissions by modest or dense shrub coverage. The effective dust source area A_{eff} stays constant throughout the year but increases linearly with a decrease of $FPAR(max_{ann})$ to a maximum of $A_{eff} = 1$ for $FPAR(max_{ann}) = 0$:

$$\text{for shrub} - \text{dominated biomes}: \quad A_{eff} = \begin{cases} 1 - FPAR(max_{ann}) & \text{if } FPAR(max_{ann}) \le 0.25 \\ 0 & \text{otherwise} \end{cases}.$$

[15] Temperate and tropical shrublands can be characterized by a mixture of shrubs and grasses. We have used the mean annual FPAR value as a criterion to treat such biomes either as grass-dominated vegetation or as shrub-dominated vegetation. Depending on the classification, the effective dust source area A_{eff} for these biomes was calculated as for grass-dominated biomes or shrub-dominated biomes (see also discussion by *Tegen et al.*, 2002]).

[16] In order to simulate the daily changes in vegetation cover, the biome-dust interface algorithm must also simulate the temporal evolution of other land-surface parameters that affect dust emission strength, specifically snow cover and soil water status. Following the approach of *Roelandt* [2001], water occurs either as snow (when the near-surface air temperature is below 0°C) or rain (when the near surface temperature is above 0°C). Snow is stored on the soil surface and only contributes water to the soil once it has melted. The soil reservoir is represented as a 15-layer cascading bucket scheme. The depth of each of these 15 buckets increases down profile from 1cm in the uppermost layer to 10 cm in the lowermost layer, such that the total depth of the soil is 1m. The available water-holding capacity of the whole soil column, as given by the BIOME4 model, is distributed between the 15 buckets proportionally to their relative size. The uppermost soil bucket is filled by precipitation. When this bucket is full, excess water is allowed to fill the underlying bucket, and when this is in turn full it will supply water to the underlying bucket until the whole soil column is saturated. Surface runoff is only allowed to occur when the whole of the soil column is saturated. Water is removed from the soil either through evaporation or by transpiration. Evaporation from the surface of the soil occurs as a function of temperature and net radiation. When the uppermost bucket is depleted, water is removed sequentially from the underlying buckets (in a simplified emulation of the process of capillary rise). Water is also removed from each bucket through transpiration. Transpiration is calculated, following *Haxeltine et al.* [1996], as the lesser of a

supply function (determined by available water in the soil) and a demand function (determined by surface air temperature and net radiation). The water uptake by plants from each soil bucket is proportional to the amount of roots present. The rooting profile with depth for different PFTs is specified following *Jackson et al.* [1996]: Arboreal PFTs have a smaller fraction of their roots in the upper soil layers while nonarboreal PFTs have a larger proportion of their roots in the upper layers.

[17] Dust deflation is inhibited when soils are wet. However, deflation is possible shortly after precipitation events because the uppermost soil layer may dry very quickly [*Gillette*, 1999]. We therefore prohibit dust deflation only if the relative soil moisture over the total soil depth, as simulated by the biome-dust interface algorithm, is greater than 99% (i.e., the soil is completely saturated). We also prohibit dust deflation from any part of a grid cell that is covered by snow. In the biome-dust interface algorithm, the snow area fraction A_{Snow} of each grid cell is estimated from simulated snow depth Sn using the relationship $A_{Snow} = Sn/(Sn + Sn_{crit})$, with a critical snow depth Sn_{crit} set to 50 mm [*Douville et al.*, 1995].

[18] To classify different soil types, seven soil texture categories with different populations of coarse sand, medium/fine sand, silt and clay (based on the FAO/UNESCO Soil Map of the World [*Zobler*, 1986]) are defined. Each of these four populations has a different mean particle diameter (coarse sand: 710 μm, medium/fine sand: 160 μm, silt: 15 μm, clay: 2 μm) and a different prescribed ratio α (m^{-1}) of vertical to horizontal soil particle flux (coarse sand: 10^{-9} m^{-1}, medium/fine sand: 10^{-8} m^{-1}, silt: 10^{-7} m^{-1}, clay: 10^{-8} m^{-1}). This definition of different soil texture categories is identical to the one used by *Tegen et al.* [2002]. Due to the lack of equivalent paleo-environmental data, we apply identical maps of soil types for the present and glacial climate simulation.

[19] Dust emission occurs from active sources when the prescribed wind speed exceeds a certain threshold velocity [*Marticorena and Bergametti*, 1995], which is dependent on soil texture. We use the approach of *Tegen et al.* [2002] to calculate the dust emission flux F:

$$F = \alpha \cdot A_{eff} \cdot (1 - A_{Snow}) \cdot G$$

with

$$G = \begin{cases} \frac{\rho_a}{g} \cdot (u^*)^3 \cdot \sum_i \left[\left(1 + \frac{u_{tr}^*(Dp_i)}{u^*}\right) \left(1 - \frac{u_{tr}^*(Dp_i))^2}{(u^*)^2}\right) \cdot s_i \right] & \text{for } u^* \geq u_{tr}^* \\ 0 & \text{otherwise} \end{cases}$$

and air density ρ_a (kgm^{-3}), gravitational constant g (ms^{-2}), surface wind velocity u* (ms^{-1}), threshold velocity u_{tr}^* (ms^{-1}) (as a function of mean diameter Dp_i), and relative surface s_i covered by each size fraction *i*. For completely saturated soils, F is set to zero.

[20] The surface wind velocities u* required to calculate dust emission fluxes were derived from 12-hour averages of the wind speed at 10m simulated by ECHAM4. As a result of their coarse spatial resolution, most AGCMs (including ECHAM4) simulate peak wind speeds considerably lower than observed [*Bengtsson et al.*, 1995]. This is likely to have a substantial impact on the simulated dust emission fluxes. In an attempt to minimize the impact of this deficiency, we derived a procedure to "correct" for this smoothing effect of the simulated wind strengths. The ECHAM monthly wind fields from the control simulation were first relaxed towards the spatially more finely resolved wind fields from the ECMWF reanalysis data (1984–1993). The ECHAM 12h wind speeds (u) were then "corrected" such that $u^* = m \cdot u + b$, with

$$m = \frac{\sigma_{ECMWF}^{mon}}{\sigma_{ECHAM}^{mon}}$$

$$b = \left(u_{ECMWF}^{mon} - u_{ECHAM}^{mon} \cdot m\right)$$

where u* is the corrected 12-hour wind speed from ECHAM4, u is the uncorrected 12-hour wind speed from ECHAM4, u_{ECHAM}^{mon} is the monthly mean wind speed from ECHAM4, σ_{ECMWF}^{mon} is the monthly mean wind speed from ECMWF, σ_{ECHAM}^{mon} is the standard deviation of the ECHAM monthly wind speed values, and σ_{ECMWF}^{mon} is the standard deviation of the ECMWF monthly wind speed values. The coefficients m and b were calculated for every grid point and every month independently. These correction values were subsequently applied to the LGM ECHAM4 wind fields.

[21] Dust transport in the atmosphere and the deposition processes are simulated using the tracer transport model TM3 [*Heimann*, 1995; The global atmospheric tracer model TM3 (model description and user manual), manuscript in preparation, 2002]. The TM3 model is run with 4° × 5° horizontal resolution, 19 vertical levels and a 12-hourly time step. Seven different size classes of dust (size class radius limits: 0.1 μm, 0.3 μm, 0.9 μm, 2.6 μm, 8 μm, 24 μm, 72 μm, 219 μm) are transported independently. Dust removal from the atmosphere occurs by dry or wet deposition. Dry deposition occurs through gravitational settling and turbulent mixing to the surface. The vertical temperature profile, required to compute the vertical extent of individual atmospheric layers from pressure coordinates and thus to calculate atmospheric sedimentation rates, is derived directly from the climate model simulation. Wet deposition occurs during convective or large-scale precipitation events. The vertical structure of precipitation is derived directly from the climate model simulation. For convective precipitation, we assume a complete washout of dust particles below the uppermost level of precipitation formation. For large-scale precipitation, the amount of dust removal is proportional to the amount of precipitation. The scavenging ratio (defined as dust concentration in precipitation divided by dust concentration in air) is set to 1000. Although this value is 25% higher than the value used by *Tegen et al.* [2002], sensitivity tests suggest that the results of our simulation of the modern dust cycle are not sensitive to the choice of scavenging ratio within a range from 750 to 1250.

2.3. Present and LGM Climate Forcing

[22] The atmospheric fields used to force the dust cycle model are derived from two 9-year-long simulations made with a recent version of the Hamburg AGCM (ECHAM4 [*Roeckner et al.*, 1996]). The model has a horizontal resolution of approximately 3.75° by 3.75° and 19 vertical levels. In the simulation of the modern climate, the mean

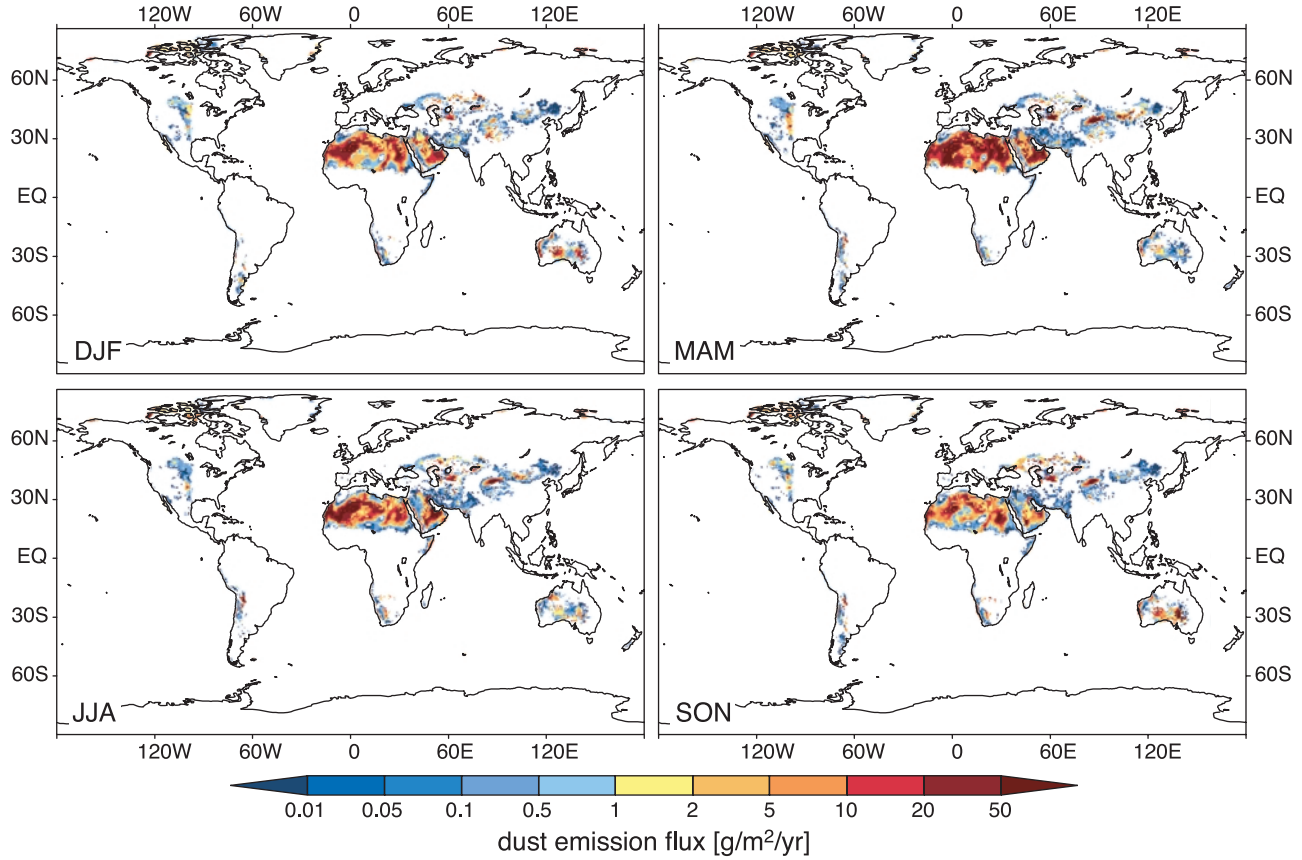

Figure 2. Simulated seasonal dust emission fluxes for the present climate using mean modern ECHAM4 atmospheric forcing fields and a prognostic biome-dust interface algorithm to predict modern vegetation coverage. The seasons are conventionally defined as December–January–February (DJF), March–April–May (MAM), June–July–August (JJA), and September–October–November (SON).

seasonal cycle of sea-surface temperatures (SSTs) and sea ice coverage averaged over the period 1979–1988 was prescribed from the Atmospheric Model Intercomparison Project (AMIP) data set and CO_2 was set to 350 ppmv. The LGM simulation was run following the Palaeoclimate Modelling Intercomparison Project (PMIP) [*Joussaume and Taylor*, 1995]) protocol, with realistic changes in the orbital configuration [*Berger*, 1978], prescribed changes in geography (including land-sea distribution and the extent and height of the ice sheets) according to *Peltier* [1994], seasonal SSTs and sea ice extent prescribed from CLIMAP [*CLIMAP Project Members*, 1981] and CO_2 set to 200 ppmv [*Barnola et al.*, 1987]. Strictly, the LGM CO_2 level should have been set to 203 ppmv (i.e. 200/345 × 350 ppmv) to conform to the PMIP protocol. However, the difference is too small to have an effect on a climate simulation made using fixed SSTs. Although the SST forcing varies seasonally, there is no change in the boundary conditions from year to year. Thus, the ECHAM4 forcing fields used to drive the dust cycle model represent the inherent variability of the atmosphere but not that of the ocean or land surface.

[23] The source and emissions schemes in the dust cycle model are run on a 0.5° by 0.5° grid. Modern and glacial atmospheric forcing fields were interpolated from the coarser ECHAM4 grid to this finer scale. The BIOME4 model is calibrated for a modern CO_2 level of 324 ppmv (corresponding to the mean CO_2 level during the years averaged to produce the modern climatology). The LGM BIOME4 simulation uses anomalies from the ECHAM4 simulations (control minus LGM) superimposed on the modern climatology (CLIMATE 2.2). In accordance with the PMIP protocol, the glacial CO_2 level was set to 188 ppmv (i.e., 200/345 × 324 ppmv) for the LGM BIOME4 run. A similar procedure was used for the biome-dust interface algorithm. The dust fluxes simulated on the 0.5° by 0.5° grid were interpolated to the coarser resolution (4° × 5°) of the TM3 tracer transport model, as were the atmospheric forcing fields (3.75° × 3.75°) required to run the tracer model. The dust cycle model was run using the full nine years of the modern simulation and the LGM simulation.

3. Results

3.1. Modern Dust Cycle

[24] Emissions from the major dust source regions in the modern simulation (Figure 2) are markedly seasonal in character. Dust emissions from Asia, including the Gobi Desert, peak in the Northern Hemisphere (NH) spring (MAM) while emissions from the southern Sahara/Sahel region peak in spring and summer (MAMJJA). In the southern hemisphere (SH), Australian emissions are maximal in SH spring (ON) and summer (DJ). Emissions from

other SH sources are rather small but nevertheless also tend to show a spring to summer peak. The emission peaks are reflected in the simulated near-surface atmospheric dust loading patterns. The timing of the simulated peak in emissions for each of the major source areas is in good agreement with regional observations of both emissions [*Orgill and Sehmel*, 1976; *Iwasaka et al.*, 1983; *Middleton et al.*, 1986; *Pye*, 1987; *Parungo et al.*, 1995], atmospheric transport patterns as seen by regional monitoring stations [*Prospero*, 1996] and satellite data [*Herman et al.*, 1997; *Husar et al.*, 1997]. According to our simulations, there is a lag of ~1 month between peak emissions and peak dust deposition at distant locations in the mid-oceans and in NH polar regions. The maximum lag appears to be in the deposition of Asian dust to Greenland, which occurs in June approximately 4–6 weeks after the peak in emissions.

[25] In our simulations, the seasonal cycle of vegetation exerts a strong control on the timing of dust emissions. Comparison of the seasonal cycle of FPAR simulated by the biome-dust interface algorithm with FPAR values derived from a 9-year average of the Normalized Difference Vegetation Index (NDVI) from the Advanced Very High Resolution Radiation (AVHRR) satellite observations [*Braswell et al.*, 1997] using the relationship FPAR = 1.222 · (NDVI/.559–0.1566) [*Knorr and Heimann*, 1995] show particularly good agreement in the location of regions of low FPAR (i.e., potential dust sources) in all seasons (Figure 3). The location and seasonality of dust sources in Africa, the Arabian Peninsula and Asia are well delineated. In Australia, the simulated FPAR values are lower than observed, particularly in winter and spring. This could lead to an overestimation of dust source areas and hence emissions in this region. The model fails to correctly simulate the high FPAR values (>80%) observed in the temperate and boreal forest zones of the NH in summer, and in the tropical rainforest and seasonal forest zones of South America in SH winter. These failures have no impact on the simulated dust cycle, since these regions never have sparse enough vegetation cover to act as dust sources. The model simulates much higher FPAR values than observed in the high latitudes of the NH during winter (Figure 3). However, the observed low values reflect probably problems in the interpretation of the AVHRR data in high-latitude regions with snow cover and nearly continuous cloud cover. Furthermore, the overestimation of vegetation cover would not significantly affect the simulation of dust emissions from high northern latitudes, where snow cover and high soil moisture throughout the winter would prevent dust deflation from taking place even in the absence of vegetation. A further measure of the realism of our simulations of the seasonal cycle of vegetation, and hence of dust emissions, is that the simulated pattern of mean dust emission fluxes agrees well with results of the simulation by *Tegen et al.* [2002], which was forced by satellite-derive observed vegetation changes and ECMWF reanalysis climate data.

[26] For the 9 years of current climate simulation, the mean total dust emission flux and standard deviation (1 σ) is 1060 ± 194 Mt/yr, integrated over the first seven bin sizes with a particle radius between 0.1 μm and 219 μm (Table 1). This value lies within the range (800–2000 Mt/yr) considered by *Tegen et al.* [2002] to be realistic. Our simulations do not include dust generated by human activities, for example cultivation, grassing, urbanization, and industrialization. First studies suggested that such activities may account for 20–50% of observed present dust emissions [*Tegen and Fung*, 1995; *Sokolik and Toon*, 1996]. However, these estimates were based on inaccurate model simulations and it is now generally assumed that the human impact effect on dust mobilization is lower. The Sahara region (20°W–32°E, 5°N–37°N) is the major source of emissions (693 ± 114 Mt/yr) in our simulation, and the simulated flux is in agreement with estimates based on observations from the region [*d'Almeida*, 1986]. Simulated emissions from the Arabian Peninsula (33°E–51°E, 5°N–37°N) are 101±40 Mt/yr, and 96±27 Mt/yr from Asia (52°E–130°E, 25°N–55°N). The emission flux from Australia (110°E–155°E, 45°S–10°S) is only 52 ± 15 Mt/yr. All these estimates are within the plausible range but poorly constrained due to a lack of direct observations [*Tegen et al.*, 2002].

[27] The largest dust deposition fluxes in the modern simulation (Figure 4a) are found close to source regions in the Sahara, Arabia, Asia and Australia. Dust emitted from the Sahara is mainly transported over tropical Atlantic regions while Asian dust is transported east towards the Pacific. These dust deposition patterns are in good agreement with the observations [e.g., *Herman et al.*, 1997; *Husar et al.*, 1997]. There are two transport routes for Australian dust: the most important carries dust northwestward into the Indian Ocean but there is also transport to the southeast towards New Zealand. Both of these pathways are apparent from observational data [*McTainsh*, 1989].

[28] Comparisons of the simulated mean dust deposition fluxes and observations from the DIRTMAP database [*Kohfeld and Harrison*, 2001] indicate that modern dust deposition fluxes in Greenland are slightly higher than observed while simulated deposition fluxes in Antarctica are substantially underestimated in our simulation (Figure 5). The underestimation of Antarctic dust deposition fluxes appears to be because ECHAM4 produces too little north-south mixing in high southern latitudes rather than any defect in our dust cycle simulation. This ECHAM4 model defect is also present in the LGM simulation and prevents dust from reaching Antarctica. Given the unrealistic simulation of both modern and LGM southern hemisphere high-latitude circulation, we do not consider Antarctica further in our analyses.

[29] The simulated dust flux to the oceans is in moderately good agreement with observed rates as measured by modern marine sediment traps (Figure 5a). The agreement is best for sites downwind from the Saharan dust plume in the midlatitude Atlantic, for sites located in the Indian Ocean, and for remote sites downwind from the main transport pathway for Asian dust in the tropical Pacific Ocean. Simulated dust fluxes close to the Asian continent are lower than observed. The simulations appear to underestimate dust fluxes as indicated by terrigenous accumulation rates from marine sediments (Figure 5b). However, sedimentation rates measured in marine sediment cores can represent very long-term averages (over the last several thousand years) because they are generally from sites with low sediment rates (~1 cm/kyr) and are sometimes based on coarse age models [see *Kohfeld and Harrison*, 2001]. Thus, a larger dispersion is to be expected amongst the dust flux measurements based on marine cores than those based on sediment traps. Despite

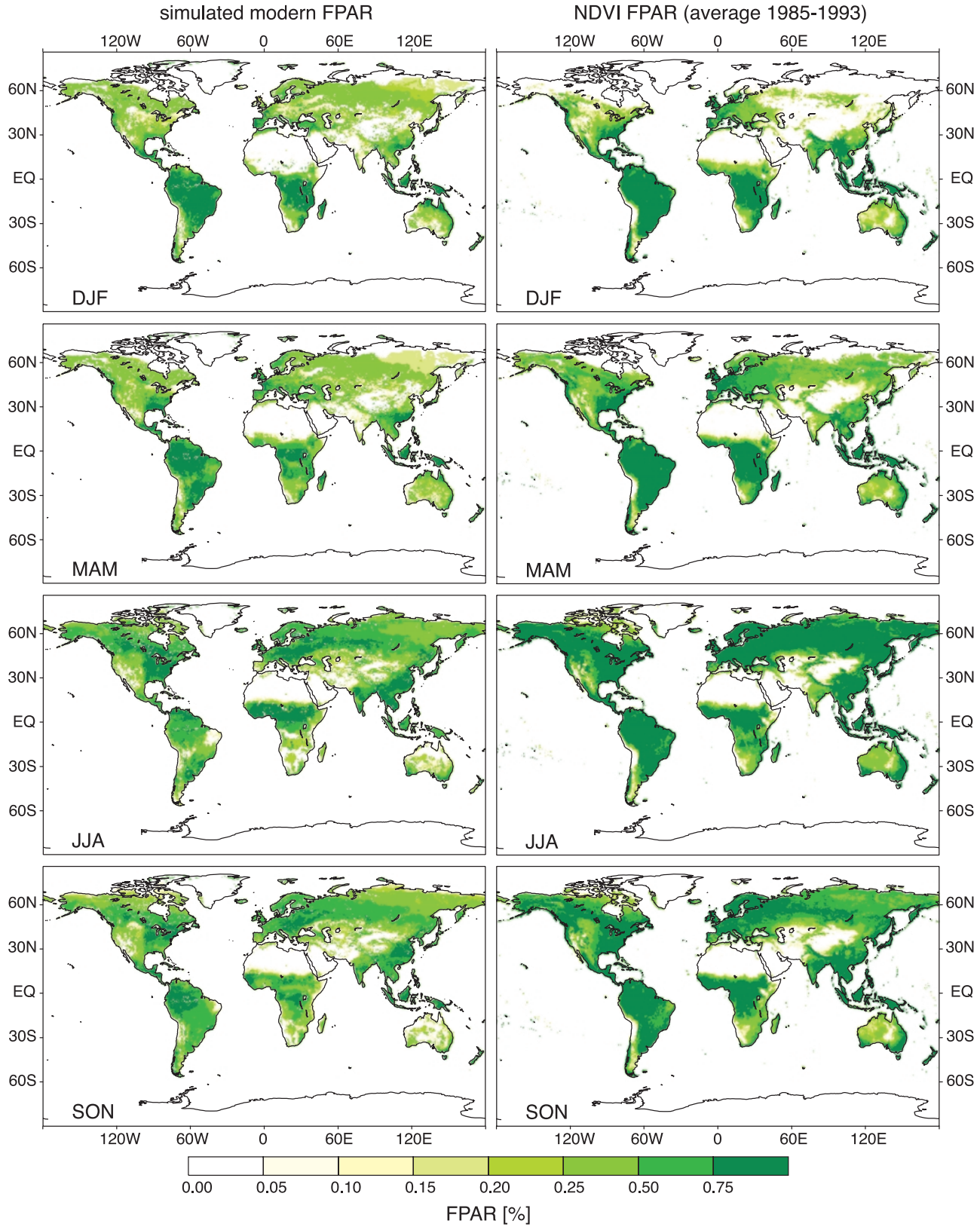

Figure 3. Comparison of the simulated modern fraction of absorbed photosynthetically active radiation (FPAR) predicted by the biome-dust interface algorithm versus the mean FPAR values derived from a 9-year average of the Normalized Difference Vegetation Index (NDVI) from the Advanced Very High Resolution Radiation (AVHRR) satellite observations. The seasons are conventionally defined, as in Figure 2.

Table 1. Mean Values and 1 σ Standard Deviation of Simulated Dust Emissions, Depositions, Atmospheric Burden and Residence Time for the Present and LGM Climate (9-Year Simulation Period)[a]

	Present	LGM	Ratio
	Emissions, Mt/yr		
Sahara	693 ± 114	1338 ± 233	1.9 (2.1)
Arabian Peninsula	101 ± 40	158 ± 33	1.6 (1.8)
Asia	96 ± 27	366 ± 70	3.8 (4.0)
Australia	52 ± 15	63 ± 12	1.2 (2.1)
High northern regions	15 ± 4	9 ± 2	0.6 (3.2)
Exposed continental shelf areas	–	304 ± 14	–
Rest	103 ± 34	146 ± 43	1.4 (2.2)
Total	**1060 ± 194**	**2383 ± 308**	**2.2**
	Depositions, Mt/yr		
61°–90°N	20 ± 4	59 ± 6	2.9
31°–60°N	143 ± 39	388 ± 84	2.7
0°–30°N	798 ± 152	1709 ± 267	2.1
0°–30°S	88 ± 16	195 ± 53	2.2
31°–60°S	6 ± 2	25 ± 4	4.3
61–90°S	0.1 ± 0.04	0.2 ± 0.2	2.7
Total	**1055 ± 193**	**2376 ± 307**	**2.3**
	Other Values		
Dry deposition, Mt/yr	811 ± 124	1716 ± 328	2.1
Wet deposition, Mt/yr	244 ± 75	660 ± 381	2.7
Atmospheric burden, Mt	**8 ± 3**	**23 ± 14**	**2.8**
Residence time, days	**2.8 ± 0.5**	**3.5 ± 1.7**	**1.3**

[a]The LGM versus present ratios are given in the far right column. For emission fluxes the ratios were calculated without taking into account the enlargement of the different LGM emission regions due to a lowered glacial sea level. The ratio in parentheses includes the emissions from adjacent, exposed continental shelf.

this, the comparison between the simulated dust fluxes and those measured on marine cores is reasonable.

[30] Comparison of the individual years of the 9-year simulation suggests that interannual differences in the emissions flux are moderate. Globally, the 1 σ standard deviation of annual fluxes is ±18% of the mean value. Interannual variability from the Sahara/Sahel is only ±17% of the mean value. Higher values are observed in Arabia (±40%) Asia (±28%) and Australia (±28%), reflecting some combination of the greater importance of interannual changes in vegetation cover in controlling the extent of active sources and higher interannual wind speed changes in these regions. There is little data that can be used to evaluate the plausibility of the simulated interannual changes, although visual examination of the TOMS aerosol index (AI) for the period 1981 through 1989 suggests that the interannual variability of AI over major source areas is generally <50%. In contrast, atmospheric dust measurements over the last 4 decades on Barbados reveal a difference in dust concentrations of a factor 4–5 between the middle to late 1960s and the early 1980s [*Prospero and Nees*, 1986]. However, such high interdecadal dust variations might be considerably influenced by ocean-atmosphere interactions on interannual to decadal timescales, like the El Niño-Southern Oscillation phenomenon, which are not captured by our model setup.

3.2. Glacial Dust Cycle

[31] Simulated global dust emission fluxes are higher by a factor 2.2 at the LGM compared to the present day and the total emissions at the LGM are 2383 ± 308 Mt/yr (Figure 6a, Table 1). The increase in emissions is largest in Asia,

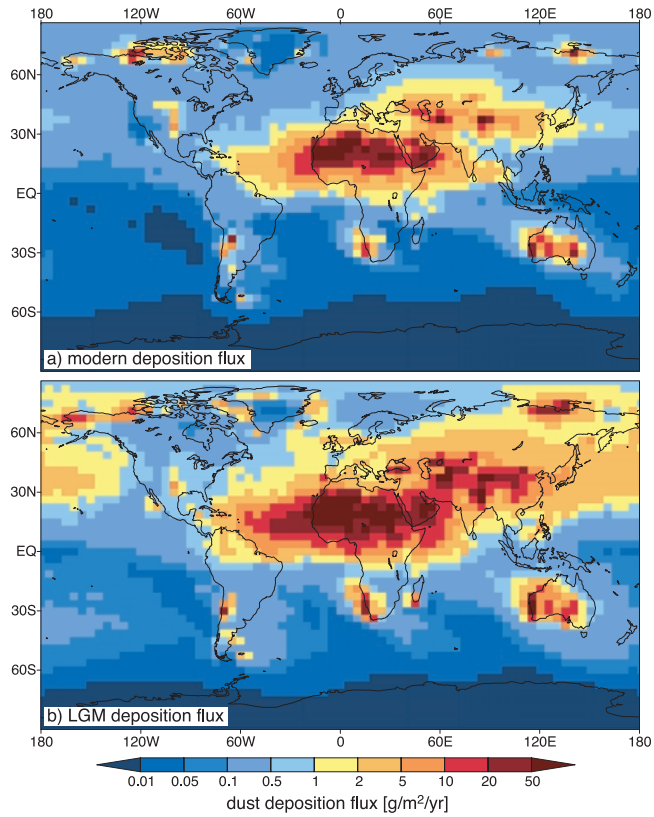

Figure 4. Simulated 9-year mean dust deposition fluxes for (a) the modern climate and (b) the LGM climate.

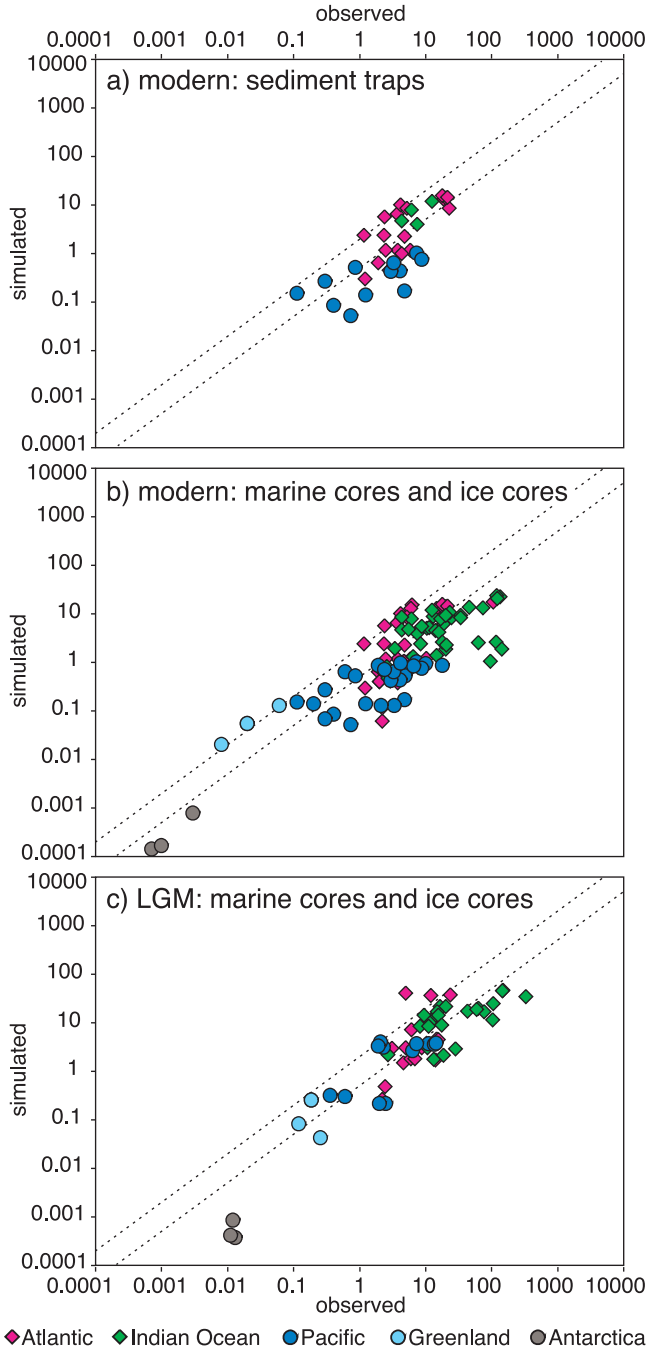

Figure 5. Comparison of simulated dust deposition fluxes (in g/m^2/yr) versus observed modern flux estimations derived from (a) marine sediment traps (log correlation coefficient is r = 0.53) and (b) marine sediment cores and ice cores (r = 0.75), and (c) LGM simulated dust deposition fluxes (in g/m^2/yr) versus observed values from marine sediment cores and ice cores (r = 0.89). In all the graphs, the dotted lines indicate a deviation of model values versus observations by a factor of ±2.

where there is an almost four-fold increase in emission fluxes. The increase in emissions is associated with an increase in the extent of dust sources in the Sahel, Asia, Australia, South Africa and South America (Table 2). Dust sources increase by ca 30% in northern Africa (Sahara), but much larger increases occur in Asia (∼50%) and Australia (∼60%). For Australia, half of the 60% increase in source area can be attributed to expanded glacial coastal areas due to the lowered glacial sea level. At the LGM, high-latitude dust source areas (north of 55°N) are 2.7-fold increased compared to the present-day climate simulation. Most of this increase is related to the extent of high-latitude coastal areas during the LGM. As a direct result, significant amounts of dust are emitted from eastern Siberia and Alaska at the LGM while there are no emissions from this region in the modern simulation.

[32] The increases in dust source areas are largely due to changes in the mean fraction of vegetation cover at the LGM (Figure 6d). To estimate the importance of this increase in glacial dust source areas versus glacial wind speed changes, a sensitivity study was performed. The model was run for 3 years (chosen to produce close to the minimum, mean and maximum dust emissions of the 9-year period) with either glacial wind speeds and modern surface conditions or vice versa (Table 3). The results suggests that approximately 25% of the simulated increase in the total global dust emission flux at the LGM is a result of the creation of source areas on the continental shelf exposed by lower sea levels at the LGM. Approximately 65% of the increase is caused by changes in wind speed over modern dust emission regions. Only 10% of the increase can be attributed to the expansion of dust sources on the modern land as a result of glacial vegetation-cover changes. However, the relative importance of vegetation changes and changes in wind speed in explaining changes in dust emissions varies from source region to source region. Changes in wind speed over modern dust emission areas appear to be the dominant factor in the Sahara/Sahel, accounting for ∼78% of the simulated increase in emissions, and in Asia (88%). Changes in vegetation cover are more important in Australia, accounting for ca 32% of the simulated increase. Australia is the only region where a decrease of emissions over modern dust regions occurs under glacial wind regimes.

[33] LGM dust deposition fluxes are increased by a factor of 2.3 compared to the present day (Figure 4b). The largest differences are found over Asia and the Northern Pacific, consistent with the three-fold increase in emissions from the Asian region. The eastward transport of Asian dust is also strongly enhanced in consequence of the stronger wind speeds in our simulation and dust deposition fluxes over the northern Pacific are much higher (× 5) than present. Increased deposition fluxes are also simulated downwind of the other source regions, including a three-fold increase in the subtropical Atlantic. The simulated regional dust deposition fluxes are in reasonable agreement with estimates of LGM dust accumulation rates from DIRTMAP (Figure 5c).

[34] The LGM atmospheric dust burden is increased by a factor of 2.8 and this leads to slight prolongation of the turnover time for dust (defined as total burden divided by deposition flux) from 2.8 ± 0.5 days under modern climate to 3.5 ± 1.7 days at the LGM (Table 1). Examination of the turnover time for different dust size bins shows that the overall increase is caused by longer atmospheric turnover times of larger dust particles (radius $\geq$ 2.6 μm) during the LGM.

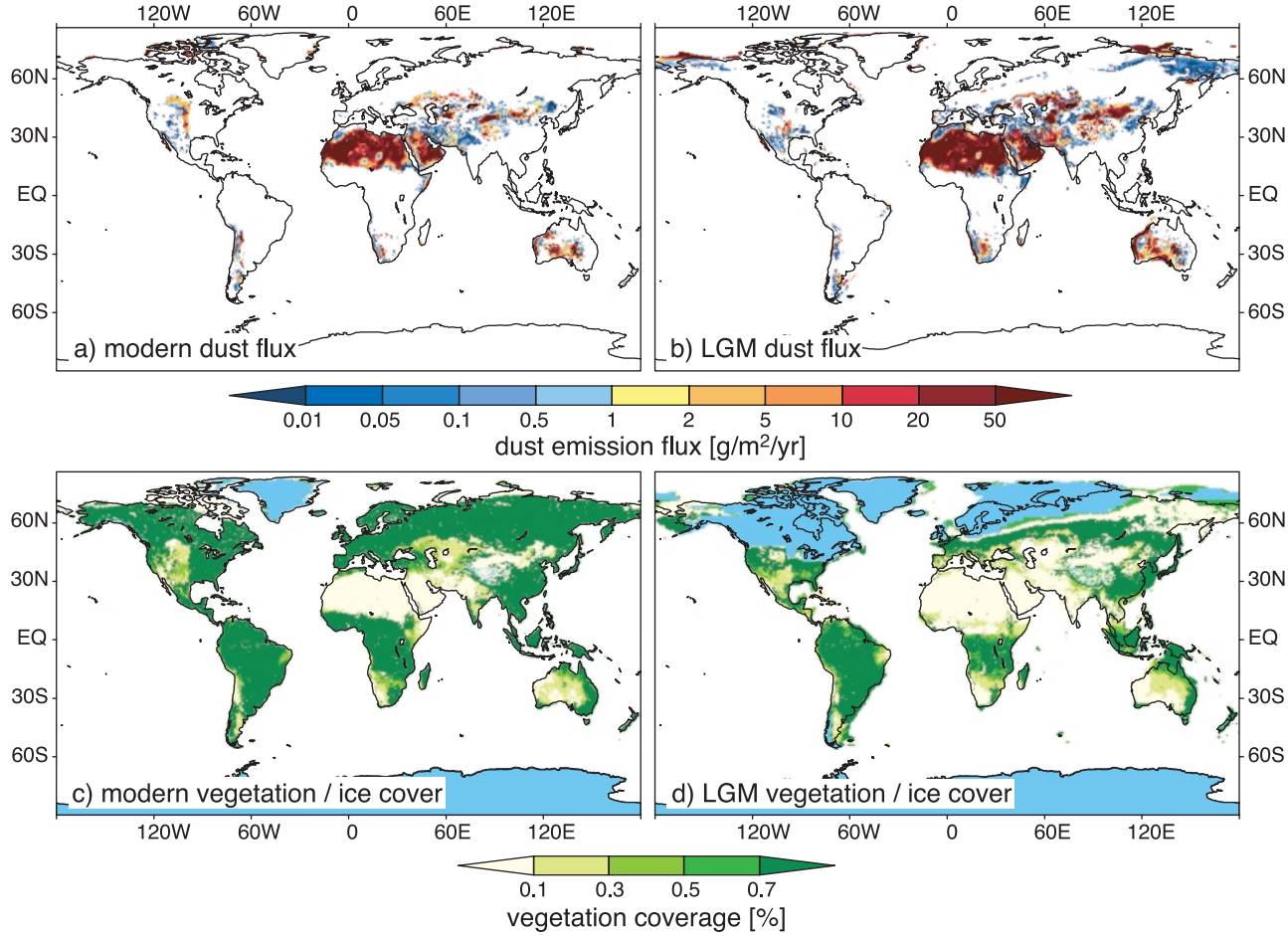

Figure 6. Simulated mean dust emission fluxes for (a) the modern and (b) the LGM climate. Simulated mean ice and vegetation cover fraction for (c) the modern and (d) the LGM climate. Ice coverage is plotted in blue in Figures 6c and 6d.

[35] The increase in the dustiness of the LGM is associated with a prolongation of the dust-emission seasons in most source regions (Figure 7) and of the season of downwind dust deposition (Figure 8). Thus, although there is a spring/summer peak (as today) in the Saharan dust plume, emissions and deposition downwind of the Sahara continue into the early autumn (September) at the LGM. The change in seasonality is very marked in central and eastern Asia. In contrast to the spring maximum in dust emission and deposition in the present-day simulation (and observations), there is an active dust cycle in the summer (July/August) at the LGM. In the high northern latitudes, which do not appear to be a significant dust source today, dust emissions and deposition are at a maximum in summer (July/August). The only exception to this general increase in the length of the season of dust activity appears to be Australia, where there is no change in the seasonality of the dust cycle compared to present.

[36] Interannual variability of emissions in the LGM global dust cycle is somewhat reduced (13%) compared to today (17%) There is no apparent change in variability over the Sahara/Sahel, but interannual variability is reduced in Australia (19% compared to 28% in the modern simulation) and in Asia (19% compared to 28% today). Interannual variability in emissions is highest on the borders of the LGM source regions, including the Sahel, parts of India, South Africa, western Australia and eastern Siberia/Alaska (Figure 9b) where the interannual variability in vegetation cover is also high (Figure 9a). However, these border regions contribute little to the total global dust emission flux (Figure 6b). Furthermore, several of these border

Table 2. Simulated Dust Emission Areas for Modern and LGM Climate Forcing[a]

Area, 10^{12} m^2	Modern	LGM
Sahara	8.2 ± 0.1	10.5 ± 0.2 (10.8 ± 0.2)
Arabian Peninsula	3.3 ± 0.0	3.9 ± 0.03 (4.2 ± 0.04)
Asia	4.6 ± 0.1	6.9 ± 0.2 (7.1 ± 0.2)
Australia	1.3 ± 0.1	1.7 ± 0.06 (2.1 ± 0.04)
High northern regions	0.4 ± 0.1	0.6 ± 0.2 (1.1 ± 0.2)
Exposed continental shelf areas	–	2.4 ± 0.0 (–)
Other sources	3.4 ± 0.2	3.7 ± 0.03 (4.5 ± 0.05)
Total	**21.2 ± 0.3**	**29.7 ± 0.5**

[a]The areas represent the simulated maximum extent of the different source regions, where dust deflation is not prohibited by any surface conditions. The number in brackets after the LGM values indicate the emission areas including sources of the adjacent, exposed continental shelf. The total emission area of exposed continental shelf acting as a dust source is also given separately.

Table 3. Results of a Sensitivity Study to Estimate the Influence of Glacial Surface Conditions and Glacial Wind Speed Changes on LGM Dust Emission Fluxes[a]

Emissions, Mt/yr	Modern Surface, Modern Winds	Modern Surface, Glacial Winds	LGM Surface, Modern Winds	LGM Surface, LGM Winds
Sahara	697 ± 149	1185 ± 211	759 ± 141	1333 ± 283
Arabian Peninsula	109 ± 66	154 ± 40	114 ± 58	164 ± 47
Asia	101 ± 51	339 ± 31	118 ± 46	372 ± 54
Australia	61 ± 18	47 ± 5	81 ± 20	62 ± 10
High northern regions	15 ± 6	39 ± 17	7 ± 3	9 ± 2
Exposed continental shelf	–	–	355 ± 27	309 ± 15
Other sources	115 ± 55	203 ± 71	116 ± 50	165 ± 78
Total	**1098 ± 326**	**1968 ± 362**	**1550 ± 324**	**2414 ± 449**

[a]Listed are mean emission and 1 σ standard deviation of a 3-year simulation period (chosen to produce close to the minimum, mean and maximum dust emissions of the modern and LGM 9-year dust simulation).

regions and most particularly those in Asia have reduced interannual climate variability (and hence dust emissions) at the LGM compared to today. Thus, the relative importance of variations in climate-induced vegetation cover on dust emissions in these border regions is less than might be expected given the importance of changes in vegetation cover in controlling dust fluxes from Asia today. Most of the interannual variability in the global dust emission flux (approximately ±308 Mt/yr) at the LGM is a result of the variability of wind speeds in the core regions, for example, the central Sahara and the Arabian Peninsula (Figures 6b and 9b). These regions are characterized by lower interannual variability than the border dust-source regions, and this also contributes towards lowering interannual variability in the dust cycle at the LGM compared to today.

[37] Our analyses indicate that the observed increase in interannual variability of dust deposition in polar regions cannot be explained by changes in the variability of emissions. Indeed, the variability of the dust emission fluxes has only relatively limited, regional impacts on global deposition fluxes (Figure 9). This is partly because the interannual changes in the deposition flux integrate the effects of variability of both the atmospheric transport and of the deposition processes themselves. Furthermore, the impact of the variability of the dust emission fluxes is further diminished by atmospheric mixing and/or the coarse resolution of the TM3 transport model. The relative importance of these two effects cannot be distinguished by our model set-up.

[38] Although interannual variability does not appear to have an important influence, changes in the seasonality of emission and deposition fluxes over the Asian region during the LGM do impact on the transport of dust to the Greenland ice sheet. The maximum dust deposition in the modern climate simulation occurs in summer (Figure 10a) which is 2–3 months later than the spring maximum dust deposition observed in the ice cores [*Steffensen*, 1988]. In the LGM simulation large dust deposition fluxes are found during most periods of the year with a clear minimum only during autumn and a much less pronounced minimum during late spring/early summer (Figure 10b). Changes in the simulated precipitation regime over Greenland, in particular a shift from a precipitation regime with no seasonal differentiation in the modern simulation to a regime with a pronounced summer maximum at the LGM, result in changes in the relative importance of wet and dry deposition. Only 28% of the dust deposited near Summit is removed by dry deposition in the modern simulation, while in the LGM simulation 76% of the dust is dry deposited.

[39] The changes in the timing of dust delivery, in the seasonality of precipitation and in the relative importance of wet and dry deposition at the LGM apparently combine to

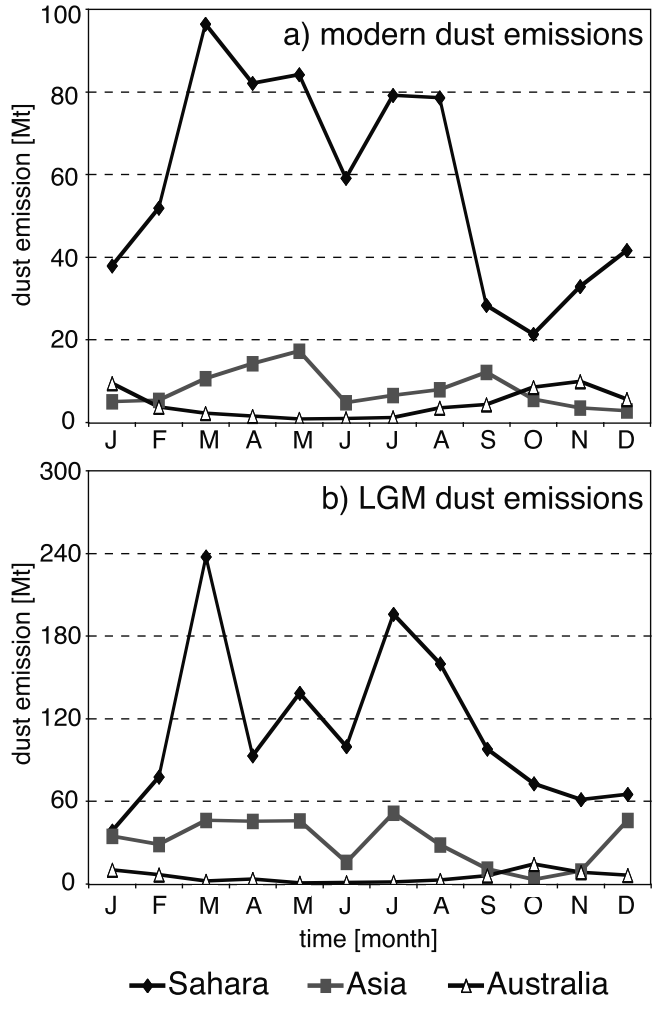

Figure 7. Mean monthly dust emission fluxes (Mt) from the Sahara/Sahel, Asia and Australia for (a) the present and (b) LGM climate. Different scales are used for the magnitude of emissions in Figures 7a and 7b.

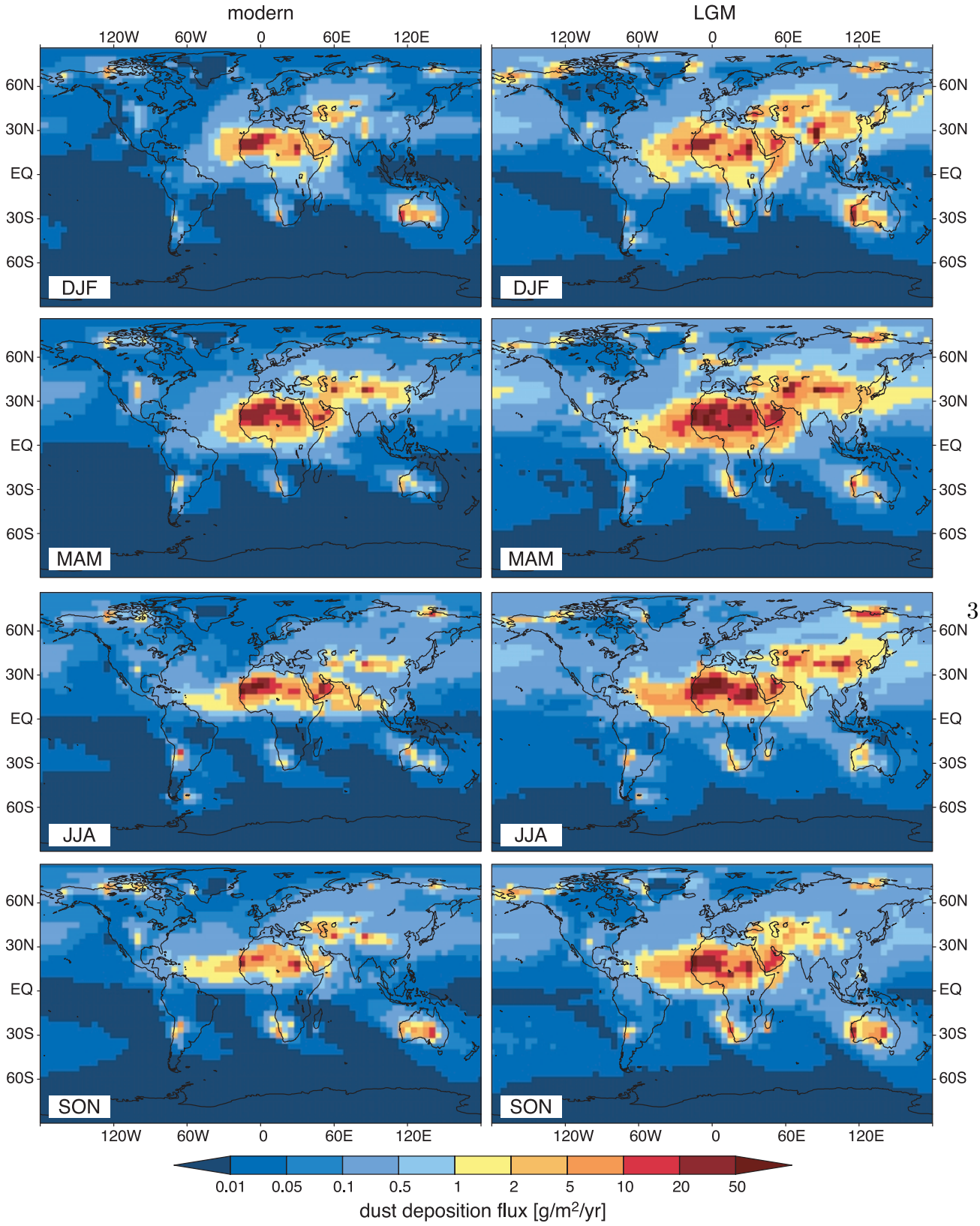

Figure 8. Mean seasonal patterns of dust deposition fluxes for (left) the modern and (right) the LGM climate. The seasons are conventionally defined, as in Figure 2.

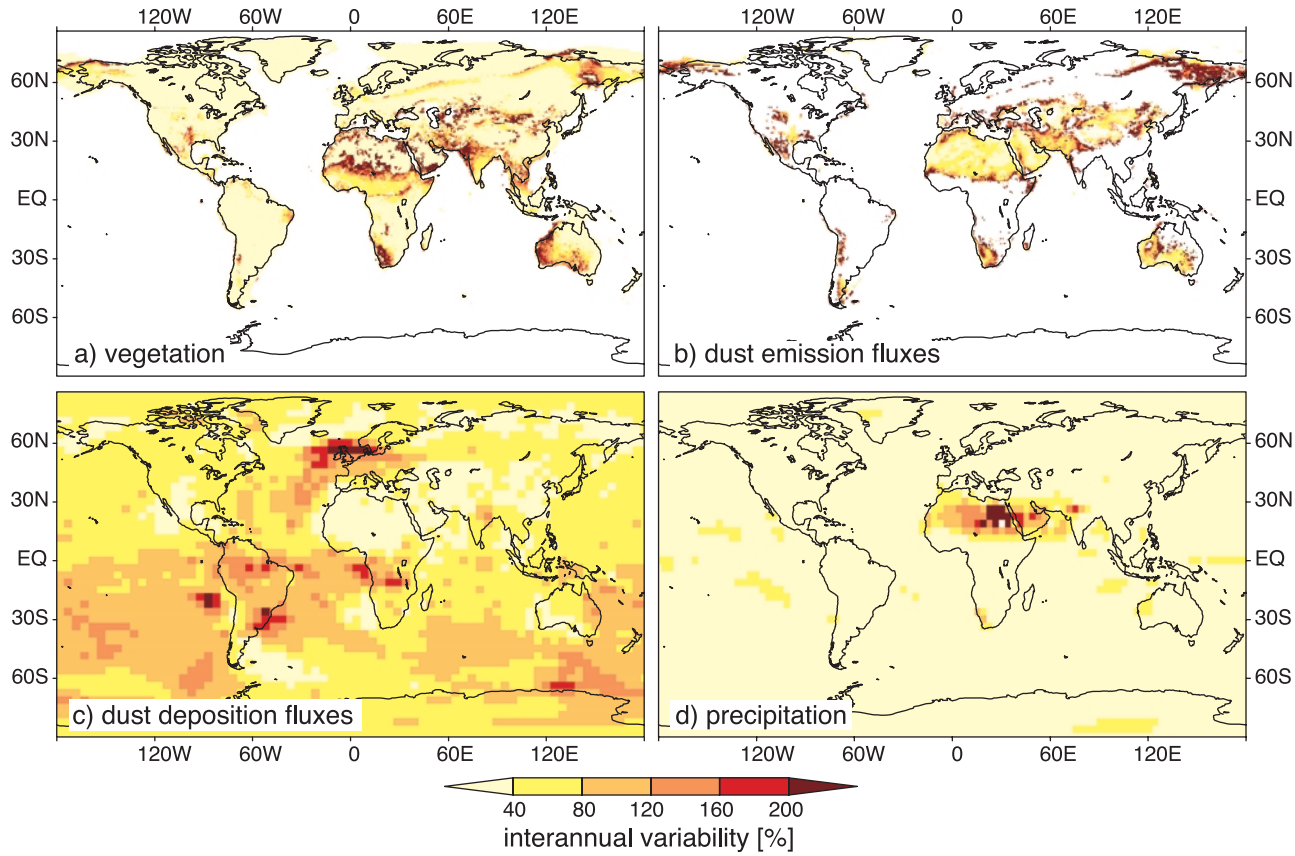

Figure 9. Simulated relative interannual variability (expressed as 1 σ standard deviation of the 9-year simulation period divided by the long-time mean value) of (a) vegetation cover changes, (b) dust emission fluxes, (c) dust deposition fluxes, and (d) precipitation during the LGM climate.

produce a considerably more spiky record of dust concentrations at the LGM than today (Figure 11): The lack of a clear seasonal cycle in modern precipitation ensures that the seasonal cycle of the simulated dust deposition flux to central Greenland translates directly into a clear seasonal cycle of dust concentrations. This is observed in many Greenland ice cores [e.g., *Steffensen*, 1988]. For the LGM, however, dust concentrations in the ice are increased by the higher glacial dust emission fluxes, reduced amount of precipitation, changed seasonality of precipitation and the increased relative importance of dry deposition processes. The combination of these effects results in very high, sharp spikes of dust concentrations. The increased interannual variability of both the glacial deposition flux and precipitation causes the high LGM dust spikes to be less evenly distributed over depth than the modern ones (Figures 11c and 11d).

4. Discussion

[40] Our simulations suggest that the total dust emission flux at the LGM was 2383 ± 308 Mt/yr, equivalent to a 2.2-fold increase in fluxes compared to present. Previous simulations of the LGM dust cycle have produced higher estimates than this, ranging from ~2700 Mt/yr [*Andersen et al.*, 1998] to 9000 Mt/yr [*Mahowald et al.*, 1999]. Both of those simulations used a tuning of the modern dust emissions by assuming a total modern dust emission flux between 2000 Mt/yr [*Andersen et al.*, 1998] and 3000 Mt/yr [*Mahowald et al.*, 1999]. Our physically based estimate of 1060 Mt/yr for the modern dust flux is lower but more plausible (see detailed discussion by *Tegen et al.* [2002]). The use of an empirical tuning of the modern fluxes in the earlier simulations should not affect the ratio of LGM to modern fluxes significantly since transport and deposition processes show an almost linear response to changes of the total emission flux. Nevertheless, our 2.2-fold increase is higher than the 1.3-fold increase reported by *Andersen et al.* [1998] and lower than the three-fold increase simulated by *Mahowald et al.* [1999].

[41] The simulated dust emission fluxes are highly dependent on the prescribed 12-hour wind speed fields. Thus, the applied wind-speed relaxation of the original ECHAM4 winds towards the ECMWF values (as described in section 2) is a crucial part of the dust modeling strategy. A sensitivity experiment with original (i.e., noncorrected) modern ECHAM4 wind fields result in an unrealistically low global dust emission flux (~600 Mt/yr), but also produces dust fluxes over parts of the Sahara and over Australia that are too high. In contrast, the use of ECMWF wind fields in the study of *Tegen et al.* [2002] yielded simulated dust emissions, which are in fair agreement with present-day observations. This agreement may justify the applied relaxation method of ECHAM4 wind speeds towards ECMWF values for the modern climate. The validity of using the same correction parameters for

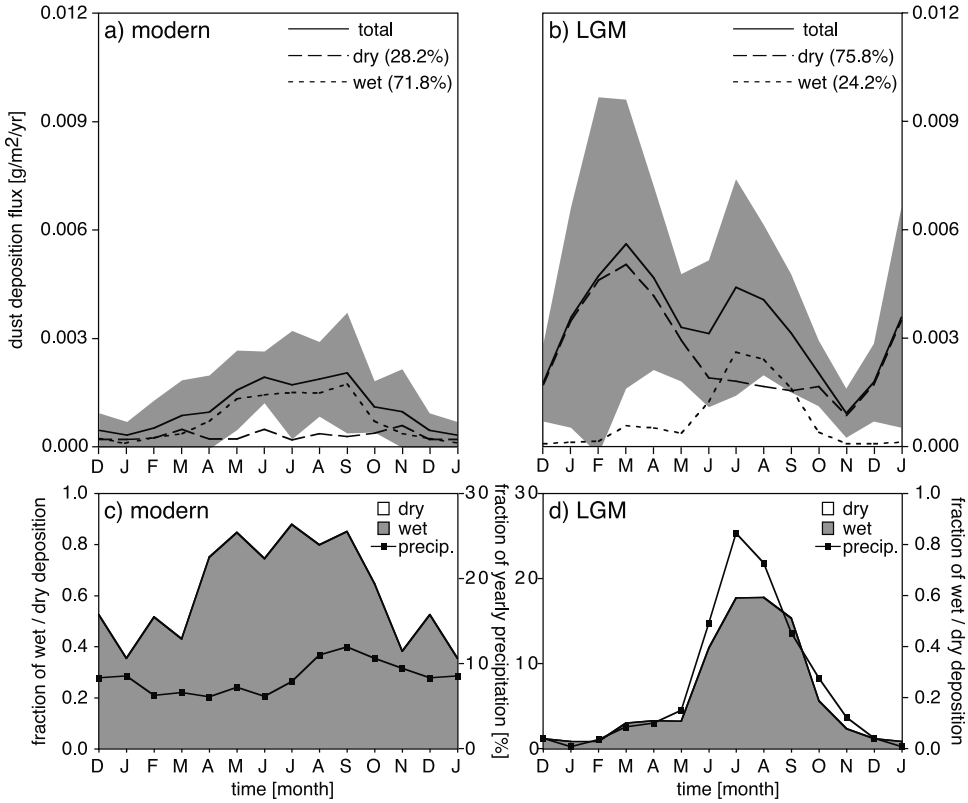

Figure 10. Simulated seasonal cycle of dust deposition near Summit, central Greenland for the (a) modern and (b) glacial climate. Mean monthly values (solid line) and the simulated 1 σ variability of the 9-year simulation period (shaded area) are shown, as are the simulated contribution of wet (short-dashed line) and dry (long-dashed line) deposition. The relative contribution of wet (shaded area) versus dry deposition (white area) and the seasonal cycle of the simulated precipitation amount (solid line with markers) for (c) modern and (d) LGM are shown. The mean December and January values are shown twice.

ECHAM4 LGM wind fields is an open question. Although there have been some attempts made to reconstruct glacial wind speeds from aeolian dune formations, these estimates only provide (at best) information on the strength of local-scale dune-forming winds. Thus, they cannot be used to test the validity of the correction parameters we use for the LGM.

[42] *Mahowald et al.* [1999] made the first attempt to account for the effects of mean glacial vegetation changes on the emission of dust particles into the atmosphere. In this study we have gone a step further by considering a more diverse distribution of biome types and by taking into account daily changes in vegetation phenology. The glacial-interglacial change in vegetation cover is somewhat reduced in our simulation compared to the changes shown by *Mahowald et al.* [1999]. The changes in vegetation cover over Africa, India and Australia are consistent with observations [*Elenga et al.*, 2000; J.-P. Sutra et al., Application of a global plant functional type scheme in the reconstruction of modern and palaeovegetation of the Indian subcontinent from pollen, manuscript in preparation, 2002; E. Pickett et al., Pollen-based reconstructions of biome distributions for Australia, South East Asia and the Pacific (SEAPAC region) at 0, 6000 and 18,000 14C yr B.P., manuscript in preparation, 2002]. The glacial high-latitudinal source region found in our simulation is also consistent with observations [*Beget*, 1996; *Edwards et al.*, 2000]. However, we appear to overestimate the extent of forests in Asia [*Yu et al.*, 2000; *Harrison et al.*, 2001] and thus probably underestimate the extent of potential dust sources in this region. Despite this, our estimates of the changes in dust emissions appear to be in better agreement with observations than previous simulations, particularly in Asia and Australia [*Kolla and Biscaye*, 1977; *Hesse*, 1994; *Kawahata*, 2002]. Glacial Australian dust emissions are increased by a factor of 2.1 compared to modern, while Asian dust emissions increased by a factor of 4.0.

[43] The seasonal cycle of vegetation changes appears to exert a strong influence on the seasonality of dust emissions in Asia, both in the modern simulation and at the LGM. Under modern conditions, interannual changes in vegetation cover on the margins of the major dust source regions influence the magnitude of dust emissions and provide an explanation for at least part of the interannual variability seen in emissions and atmospheric dust loadings. The largest impacts seem to be registered in Asia, southern Africa and Australia. However, given that the contribution of these border zones to the overall magnitude of dust emitted from each source is small, interannual changes in vegetation cover are not the most important control on either the total dust flux or its variability under modern conditions. The interannual variability of vegetation cover

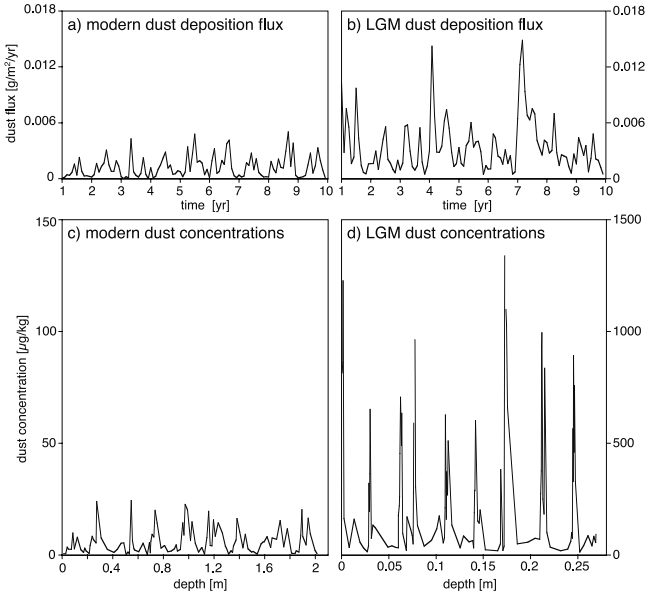

Figure 11. Simulated monthly deposition fluxes plotted versus time near Summit, Greenland, for the 9 years of (a) modern and (b) LGM climate, and simulated monthly dust concentrations in the snow plotted versus depth for (c) modern and (d) LGM climate. Dust concentrations were calculated as total dust deposition flux divided by precipitation amount. Depth was calculated by accumulating the precipitation amounts (sublimation of snow or post-depositional wind effects were neglected). Note the different dust concentration scales for the modern climate (Figure 11c) and the LGM climate (Figure 11d).

appears to have been reduced at the LGM, and thus its impact on the total dust emission would have been further reduced. Our simulations show that the increased strength and increased variability of glacial winds are the most important factors explaining the enhanced dust cycle at the LGM. This is particularly true for the Sahara/Sahel and Asia, where changes in the glacial winds explain ~78% and ~88% of the increase in dust emissions, respectively. Only in Australia, vegetation appears to be relatively more important in explaining the glacial changes. *Mahowald et al.* [1999] also showed that the increase in emissions from the Sahara at the LGM (compared to present) was largely controlled by increased wind speeds rather than vegetation changes. However, they argued that changes in other regions were dependent on the increased extent of source areas due to climatically-controlled changes in the extent of vegetation. Our results suggest that even rather large changes in potential source areas, such as the 50% increase simulated in Asia, may have little impact on total emissions.

[44] Ice cores information from Greenland and Antarctica currently provide the only reliable source of information about interannual variability of dust concentrations. *Fuhrer et al.* [1999] reported order-of-magnitude changes of the calcium concentration of the Greenland GRIP ice core in about a decade, with 50% reductions within 2–3 years. The authors invoke a combination of increased atmospheric residence times and increased dust mobilization from Asia as the most plausible explanations for these rapid changes but, on the basis of earlier model studies [*Alley et al.*, 1995; *de Angelis et al.*, 1997], dismiss the possibility that the changes in dust concentration could be influenced by changes in the relative importance of wet and dry deposition. Our simulation suggests changes in the seasonality of precipitation and increases in the importance of dry deposition both have a substantial impact on the very rapid, short-term dust concentration changes found in central Greenland ice cores during the LGM. The increased seasonality of LGM precipitation over Greenland compared to present has also been found in other AGCM simulations [e.g., *Krinner et al.*, 1997].

[45] *Unnerstad and Hansson* [2001], on the basis of observed dust concentrations, aerosol size distributions, precipitation rates and a simple deposition model, estimated dry deposition accounted for 5%–25% of the total dust deposition today and between 13%–41% of the deposition during the LGM at the GRIP ice core. The two-fold increase in the dry deposition fraction during the LGM is broadly consistent with our estimate of a 2.7-fold increase (modern dry fraction: 28%, glacial dry fraction: 76%). The difference between the studies probably results from differences in the LGM precipitation rates used (Unnerstad and Hansson: 9 cm/yr, this study: 3 cm/yr) or could reflect the fact that *Unnerstad and Hansson* [2001] do not take into account the seasonality of atmospheric transport and precipitation.

[46] *Hansson* [1994] suggested that prolonged glacial residence times could explain the increasing LGM dust fluxes and concentrations in Greenland ice cores. Our simulation results suggest a slight increase in residence time during the LGM on a global scale. However, this increase in residence time is only caused by larger dust particles, which are rarely transported to remote regions, like Greenland and therefore do not substantially affect the LGM dust record in Greenland ice cores.

[47] The isotopic composition of glacial dust found in the GISP2 ice core has been interpreted to indicate that the most likely source of glacial dust deposited in central Greenland is the Gobi desert and China [*Biscaye et al.*, 1997]. In a 1-year sensitivity experiment (chosen to produce close to the mean dust emissions) we tagged the dust emission fluxes from different source regions. In both the present and glacial simulation, several source regions contribute significantly to the modeled dust deposition flux near Summit, central Greenland. The combined Asian and Caspian Sea region is the most important source location, accounting for 35% (modern) and 42% (LGM) of the total central Greenland dust flux. While these findings agree with the conclusions of *Biscaye et al.* [1997] that Asia is the most important dust source for glacial dust found in central Greenland ice cores, they emphasize that other sources could also make a significant contribution to the Greenland dust deposition.

[48] An overestimation of the absolute values of high glacial dust concentration peaks in our simulation cannot be excluded since any post-depositional effects (e.g., relayering of the uppermost snow) were neglected. However, such mechanisms should reduce both modern and glacial dust spikiness in a similar manner.

[49] Aerosol records other than dust (e.g., sea salt, sulphate) show strong, rapid variations in the Greenland ice-core records during cold climate stages [e.g., *Hansson*, 1994]. These variations may also reflect a shift in the

seasonality of glacial precipitation and the strong increase of the relative importance of dry deposition processes that we invoke as an explanation of the variability of dust records in ice cores during the LGM. Wet deposition of all aerosol species would be inhibited during glacial winter, resulting in either enhanced dry deposition (which would raise concentration levels in the surface snow) or the build-up of aerosol loads in the atmosphere (leading to higher wet deposition fluxes during subsequent precipitation events). Our results indicate that such a shift of the relative importance of dry deposition processes during the LGM is not confined to Greenland, but occurs over most areas north of 60°N. No changes of the wet to dry deposition ratio are found in midlatitudinal and subtropical regions in the LGM simulation.

[50] The robustness of our results will be influenced by the correctness of the simulated LGM climate. The ECHAM4 simulation for the LGM followed the PMIP protocol in specifying ice sheet extent and height from *Peltier* [1994] and sea-surface conditions (both sea-surface temperatures and sea-ice extent) from CLIMAP [*CLIMAP Project Members*, 1981]. Recent work suggests that certain aspects of both of these data sets may be unrealistic.

[51] Recent reconstructions of tropical SSTs, based on alkenone unsaturation ratios [*Ohkouchi et al.*, 1994; *Zhao et al.*, 1995; *Chapman et al.*, 1996; *Bard et al.*, 1997; *Rosell-Melé et al.*, 1998; *Sonzogni et al.*, 1998], oxygen-isotopes [*Lee and Slowey*, 1999] or modern-analog analyses of new (or extended) biotic assemblage data sets [*Guilderson et al.*, 1994; *Wolff et al.*, 1998; *Mix et al.*, 1999; *Liu et al.*, 2000] indicate that the tropical oceans were cooler than shown by CLIMAP [*CLIMAP Project Members*, 1981]. Conversely, reconstructions based on both dinoflagellate cysts [*De Vernal et al.*, 1997; *Rochon et al.*, 1998; *de Vernal and Hillaire-Marcel*, 2000] and foraminiferal assemblages [*Weinelt et al.*, 1996] indicate that the North Atlantic was warmer during the summer season than shown by CLIMAP. All PMIP simulations using CLIMAP SSTs underestimate the observed tropical cooling, and most of the models also underestimate the extent of glacial aridity across the tropics [*Pinot et al.*, 1999a]. Both effects would most likely lead to a reduced vegetation cover in those areas. Thus we might expect our simulation to underestimate LGM dust emissions in tropical regions. Evaluations using pollen-based reconstructions of temperature and moisture balance parameters across Europe and Russia suggest that the underestimation of tropical SSTs at the LGM in the PMIP simulations results in the simulation of climates across western and central Europe, and the eastern Mediterranean, that are too warm and wet [*Kageyama et al.*, 2001]. These regions are not major dust sources in our LGM simulation. However, if climate were drier than simulated (as shown by the pollen data), we might expect significant dust sources to be created. Thus, we expect our simulations to underestimate dust emissions from southern and central Europe as a result of the prescription of CLIMAP SSTs in the tropics. In contrast, it would appear that the use of CLIMAP SSTs in the North Atlantic is unlikely to have a significant effect on our simulation of the LGM dust cycle. Sensitivity experiments with two versions of the LMD AGCM suggest that the impact of a warmer North Atlantic during the LGM summer is restricted to creating warmer conditions in eastern North America, Europe north of the Mediterranean region, and western Siberia [*Pinot et al.*, 1999b]. The warmer North Atlantic does not appear to impact on the hydrological cycle, and thus can be expected to have little or no effect on the area of dust sources in the midlatitudes.

[52] The *Peltier* [1994] reconstruction of the LGM ice sheets shows the European ice sheet as more extensive than it was in reality [*Astakhov et al.*, 1999]. Furthermore, according to the *Peltier* [1994] reconstruction the Greenland ice sheet is ~500 m higher than today, whereas recent reconstructions suggest there was little difference in the height of the Greenland ice sheet from today [*Cuffey and Clow*, 1997]. The impact of ice over western and northern Siberia on the simulated climate and dust cycle at the LGM is uncertain. On one hand, the unrealistically extended ice sheet would limit the possible extent of high-latitude sources and thus reduce possible emissions. However, the magnitude and spatial extent of glacial cooling and aridity downwind from the European ice sheet is at least partially influenced by the extent of the ice sheet. Thus, the prescription of an unrealistically large ice sheet would result in colder and drier conditions in the high-northern latitudes, thus creating more extensive potential dust sources. The balance between these two effects cannot be determined without running new climate simulations. The impact of the incorrect specification of the height of the Greenland ice sheet has, however, been evaluated. When the Greenland ice sheet at the LGM is specified according to Peltier's reconstruction, the simulated mean precipitation is only ~3 cm/yr in central Greenland. This is 1.5–6 cm/yr lower than estimates of the LGM precipitation derived from the GRIP and GISP2 ice cores [*Johnsen et al.*, 1995; *Cuffey and Clow*, 1997]. Reducing the change in elevation of the LGM Greenland ice sheet by 400 m results in a more realistic simulation of the LGM precipitation in central Greenland [*Werner et al.*, 2000]. However, neither imposing a more realistic Greenland ice sheet nor more realistic SSTs in the North Atlantic and in the tropics substantially affects the simulated seasonality of precipitation on Greenland [*Werner et al.*, 2001]. Our results invoke a change in the seasonality and interannual variability of precipitation to explain the extreme variability in dust concentration seen in the Greenland ice cores during the glacial, and thus our conclusions are unaffected by the use of the Peltier reconstruction of the ice sheets.

[53] Mineral aerosols play multiple roles in the climate system, including changing the radiative balance of the atmosphere [*Intergovernmental Panel on Climate Change*, 2001], influencing the physical properties of clouds [*Levin et al.*, 1996; *Zhang and Carmichael*, 1999; *Wurzler et al.*, 2000], and acting as a source of micronutrients to marine [*Martin*, 1991; *Coale et al.*, 1996; *Hutchins and Bruland*, 1998] and terrestrial [*Swap et al.*, 1992; *Chadwick et al.*, 1999] ecosystems. The change in the radiative balance of the atmosphere caused by the increased glacial atmospheric dust loads could be substantial in tropical and subtropical regions [*Claquin et al.*, 2002]. Recent simulations suggest that the impact of glacial fertilization of marine ecosystems was rather small, although nonnegligible [*Bopp*, 2001]. Given that these feedbacks can occur rather rapidly (i.e., on subannual to decadal timescales), they may influence the interannual variability of climate (and hence of the dust

cycle) as well as the mean climate state of the LGM. Determining how these feedbacks will impact on the LGM dust cycle, however, will require coupling a dust sources, emission, transport and deposition scheme, such as the offline scheme used here, into a climate model.

5. Conclusions

[54] Our simulations of the atmospheric dust cycle with prescribed modern and LGM boundary conditions show the following.

1. There is a two- to three-fold increase of the global atmospheric dust load during the LGM compared to modern. This is in general agreement with previous studies. However, our improved dust emission scheme indicates substantially lower absolute values of total dust emissions for both modern and LGM climate.

2. One third of the simulated increase in the total global dust emission flux at the LGM is related to source-region changes, while two thirds is caused by glacial wind speed changes over modern dust emission regions.

3. The season of dust emission for most source regions is longer in the LGM climate simulation than in the modern simulation. In particular in central Asia strong glacial dust emissions were simulated from early winter through to late summer in contrast to the clear modern spring maximum.

4. A substantial increase in the importance of dry deposition processes is found for most northern high-latitude regions during the LGM.

5. Changes in LGM dust emissions would only produce relatively small changes in dust deposition in Greenland. The very large observed changes in dust concentrations in Greenland ice cores can only be explained by taking into account changes in the seasonal cycle of both dust emission and of precipitation.

[55] **Acknowledgments.** This paper is a contribution to the MAGIC (Mineral Aerosols and Glacial-Interglacial Cycles) project, originally funded by the Swedish Natural Research Council (NFR) and now supported by the Max-Planck-Institute for Biogeochemistry. M. Werner, K. E. Kohfeld, and C. Roelandt were all originally supported as postdoctoral scientists by the NFR; this support is gratefully acknowledged. We thank Kerstin Sickel for assistance with the BIOME4 simulations and Wolfgang Cramer for providing the CLIMATE2.2 data set. The ECHAM4 simulations were performed with support from the German Climate Computing Center (DKRZ) in Hamburg, Germany. The constructive comments and criticisms from two anonymous reviewers helped us improving our manuscript and are greatly appreciated.

References

Alley, R., R. C. Finkel, K. Nishiizumi, S. Anandakrishnan, C. A. Shuman, G. R. Mershon, G. A. Zielinski, and P. A. Mayewski, Changes in continental and sea-salt atmospheric loadings in central Greenland during the most recent deglaciation: Model-based estimates, *J. Glaciol.*, *41*, 503–514, 1995.

Andersen, K. K., A. Armengaud, and C. Genthon, Atmospheric dust under glacial and interglacial conditions, *Geophys. Res. Lett.*, *25*(13), 2281–2284, 1998.

Astakhov, V. I., J. I. Svendsen, A. Matiouchkov, J. Mangerud, O. Maslenikova, and J. Tveranger, Marginal formations of the last Kara and Barents ice sheets in northern European Russia, *Boreas*, *28*(1), 23–45, 1999.

Bard, E., F. Rostek, and C. Sonzogni, Interhemispheric synchrony of the last deglaciation inferred from alkenone palaeothermometry, *Nature*, *385*, 707–710, 1997.

Barnola, J. M., D. Raynaud, Y. S. Korotkevich, and C. Lorius, Vostok ice core provides 160,000-year record of atmospheric CO2, *Nature*, *329*, 408–414, 1987.

Beget, J. E., Tephrochronology and paleoclimatology of the last interglacial-glacial cycle recorded in Alaskan loess deposits, *Quat. Int.*, *34*(6), 121–126, 1996.

Bengtsson, L., M. Botzet, and M. Esch, Hurricane-type vortices in a general circulation model, *Tellus, Ser. A*, *47*, 175–196, 1995.

Berger, A. L., Long-term variations of daily insolation and Quarternary climatic changes, *J. Atmos. Sci.*, *35*, 2362–2367, 1978.

Biscaye, P. E., F. E. Grousset, M. Revel, S. Vandergaast, G. A. Zielinski, A. Vaars, and G. Kukla, Asian provenance of glacial dust (stage 2) in the Greenland Ice Sheet Project 2 ice core, Summit, Greenland, *J. Geophys. Res.*, *102*(C12), 26,765–26,781, 1997.

Bopp, L., Changements climatiques et biogéochimie océanique, Ph.D. thesis, 318 pp., Univ. Pierre et Marie Curie, Paris, France, 2001.

Braswell, B. H., D. S. Schimel, E. Linder, and B. Moore, The response of global terrestrial ecosystems to interannual temperature variability, *Science*, *278*, 870–872, 1997.

Chadwick, O. A., L. A. Derry, P. M. Vitousek, B. J. Huebert, and L. O. Hedin, Changing sources of nutrients during four million years of ecosystem development, *Nature*, *397*, 491–497, 1999.

Chapman, M. R., N. J. Shackleton, M. Zhao, and G. Eglinton, Faunal and alkenone reconstructions of subtropical North Atlantic surface hydrography and paleotemperature over the last 28 Kyr, *Paleoceanography*, *11*(3), 343–357, 1996.

Claquin, T., et al., Radiative forcing of climate by ice-age atmospheric dust, *Clim. Dyn.*, in press, 2002.

CLIMAP Project Members, Seasonal reconstruction of the Earth surface at the Last Glacial Maximum, *Map and Chart. Ser. MC-36*, Geol. Soc. of Am., Boulder, Colo., 1981.

Coale, K. H., et al., A massive phytoplankton bloom induced by an ecosystem-scale iron fertilization experiment in the Equatorial Pacific Ocean, *Nature*, *383*, 495–501, 1996.

Coe, M. T., A linked global model of terrestrial hydrologic processes: Simulation of modern rivers, lakes, and wetlands, *J. Geophys. Res.*, *103*(D8), 8885–8899, 1998.

Cuffey, K. M., and G. D. Clow, Temperature, accumulation, and ice sheet elevation in central Greenland through the last deglacial transition, *J. Geophys. Res.*, *102*(C12), 26,383–26,396, 1997.

d'Almeida, G. A., A model for Saharan dust transport, *J. Clim. Appl. Meteorol.*, *25*(7), 903–916, 1986.

de Angelis, M., J. P. Steffensen, M. Legrand, H. Clausen, and C. Hammer, Primary aerosol (sea salt and soil dust) deposited in Greenland ice during the last climatic cycle: Comparison with East Antarctic records, *J. Geophys. Res.*, *102*(C12), 26,681–26,698, 1997.

de Vernal, A., and C. Hillaire-Marcel, Sea-ice cover, sea-surface salinity and halo-/thermocline structure of the northwest North Atlantic: Modern versus full glacial conditions, *Quat. Sci. Rev.*, *19*, 65–85, 2000.

de Vernal, A., A. Rochon, J. L. Turon, and J. Matthiessen, Organic-walled Dinoflagellate cysts-Palynological tracers of sea-surface conditions in middle to high latitude marine environments, *Geobios*, *30*(7), 905–920, 1997.

Douville, H., J. F. Royer, and J. F. Mahfouf, A new snow parameterization for the Meteo-France climate model: Validation in stand-alone experiments, *Clim. Dyn.*, *12*(1), 21–35, 1995.

Edwards, M. E., et al., Pollen-based biomes for Beringia 18,000, 6000 and 0 C-14 yr BP, *J. Biogeogr.*, *27*(3), 521–554, 2000.

Elenga, H., et al., Pollen-based biome reconstruction for southern Europe and Africa 18,000 yr BP, *J. Biogeogr.*, *27*(3), 621–634, 2000.

Food and Agriculture Organization, Digital soil map of the world and derived soil properties, report, Rome, 1995.

Fuhrer, K., E. W. Wolff, and S. J. Johnsen, Timescales for dust variability in the Greenland Ice Core Project (GRIP) ice core in the last 100,000 years, *J. Geophys. Res.*, *104*(D24), 31,043–31,052, 1999.

Genthon, C., and A. Armengaud, GCM simulations of atmospheric tracers in the polar latitudes-South Pole (Antarctica) and Summit (Greenland) cases, *Sci. Total Environ.*, *161*, 101–116, 1995.

Gillette, D. A., A qualitative geophysical explanation for "hot spot" dust emitting source regions, *Contrib. Atmos. Phys.*, *72*, 67–77, 1999.

Ginoux, P., M. Chin, I. Tegen, J. M. Prospero, B. Holben, O. Dubovik, and S. J. Lin, Sources and distributions of dust aerosols simulated with the GOCART model, *J. Geophys. Res.*, *106*(D17), 20,255–20,273, 2001.

Guilderson, T. P., R. G. Fairbanks, and J. L. Rubenstone, Tropical temperature variations since 20,000 years ago: Modulating interhemispheric climate change, *Science*, *263*, 663–665, 1994.

Hansson, M. E., The Renland ice core-A Northern Hemisphere record of aerosol composition over 120,000 years, *Tellus, Ser. B*, *46*, 390–418, 1994.

Harrison, S. P., G. Yu, H. Takahara, and I. C. Prentice, Diversity of temperate plants in East Asia, *Nature*, *413*, 129–130, 2001.

Haxeltine, A., I. C. Prentice, and I. D. Creswell, A coupled carbon and water flux model to predict vegetation structure, *J. Veg. Sci.*, *7*(5), 651–666, 1996.

Heimann, M., The global atmospheric tracer model TM2 (model description and user manual), *Tech. Rep. 10*, 47 pp., Deutsches Klimarechenzentrum, Hamburg, Germany, 1995.

Herman, J. R., P. K. Bhartia, O. Torres, C. Hsu, C. Seftor, and E. Celarier, Global distribution of UV-absorbing aerosols from Nimbus 7/TOMS data, *J. Geophys. Res.*, *102*(D14), 16,911–16,922, 1997.

Hesse, P. P., The record of continental dust from Australia in Tasman Sea sediments, *Quat. Sci. Rev.*, *13*, 257–272, 1994.

Hu, F. S., D. Slawinski, H. E. Wright, E. Ito, R. G. Johnson, K. R. Kelts, R. F. McEwan, and A. Boedigheimer, Abrupt changes in North American climate during early Holocene times, *Nature*, *400*, 437–440, 1999.

Husar, R. B., J. M. Prospero, and L. L. Stowe, Characterization of tropospheric aerosols over the oceans with the NOAA advanced very high resolution radiometer optical thickness operational product, *J. Geophys. Res.*, *102*(D14), 16,889–16,909, 1997.

Hutchins, D. A., and K. W. Bruland, Iron-limited diatom growth and Si/N uptake ratios in a coastal upwelling regime, *Nature*, *393*, 561–564, 1998.

Intergovernmental Panel on Climate Change, *Climate Change 2001: The Scientific Basis: Contribution of Working Group I to The Third Assessment Report of the Intergovernmental Panel on Climate Change*, edited by J. T. Houghton et al., 881 pp., Cambridge Univ. Press, New York, 2001.

Iwasaka, Y., H. Minoura, and K. Nagaya, The transport and spatial scale of Asian dust-storm clouds-A case-study of the dust-storm event of April 1979, *Tellus, Ser. B*, *35*, 189–196, 1983.

Jackson, R. B., J. Canadell, J. R. Ehleringer, H. A. Mooney, O. E. Sala, and E. D. Schulze, A global analysis of root distributions for terrestrial biomes, *Oecologia*, *108*(3), 389–411, 1996.

Johnsen, S. J., D. Dahl-Jensen, W. Dansgaard, and N. S. Gundestrup, Greenland paleotemperatures derived from GRIP bore hole temperature and ice core isotope profiles, *Tellus, Ser. B*, *47*, 624–629, 1995.

Joussaume, S., Three-dimensional simulation of the atmospheric cycle of desert dust particles using a general circulation model, *J. Geophys. Res.*, *95*(D2), 1909–1941, 1990.

Joussaume, S., and K. E. Taylor, Status of the Paleoclimate Modelling Intercomparison Project (PMIP), in *First International AMIP Scientific Conference*, pp. 425–430, World Clim. Res. Programme, Geneva, 1995.

Kageyama, M., O. Peyron, S. Pinot, P. Tarasov, J. Guiot, S. Joussaume, and G. Ramstein, The Last Glacial Maximum climate over Europe and western Siberia: A PMIP comparison between models and data, *Clim. Dyn.*, *17*(1), 23–43, 2001.

Kaplan, J. O., Geophysical applications of vegetation modeling, Ph.D. thesis, Dep. of Ecol., Lund Univ., Lund, Sweden, 2001.

Kawahata, H., Shifts in oceanic and atmospheric boundaries in the Tasman Sea (Southwest Pacific) during the late Pleistocene: Evidence from organic carbon and lithogenic fluxes, *Palaeogeogr. Palaeoclimatol. Palaeoecol.*, *2771*, 1–25, 2002.

Knorr, W., and M. Heimann, Impact of drought stress and other factors on seasonal land biosphere CO2 exchange studied through an atmospheric tracer transport model, *Tellus, Ser. B*, *47*, 471–489, 1995.

Kohfeld, K. E., and S. P. Harrison, DIRTMAP: The geological record of dust, *Earth Sci. Rev.*, *54*, 81–114, 2001.

Kolla, V., and P. E. Biscaye, Distribution and origin of quartz in sediments of Indian ocean, *J. Sediment. Petrol.*, *47*(2), 642–649, 1977.

Krinner, G., C. Genthon, and J. Jouzel, GCM analysis of local influences on ice core delta signals, *Geophys. Res. Lett.*, *24*(22), 2825–2828, 1997.

Lee, K. E., and N. C. Slowey, Cool surface waters of the subtropical North Pacific Ocean during the last glacial, *Nature*, *397*, 512–514, 1999.

Levin, Z., E. Ganor, and V. Gladstein, The effects of desert particles coated with sulfate on rain formation in the Eastern Mediterranean, *J. Appl. Meteorol.*, *35*(9), 1511–1523, 1996.

Liu, Z., S. Shin, P. Behling, W. Prell, M. Trend-Staid, S. P. Harrison, and J. E. Kutzbach, Dynamical and observational constraints on tropical Pacific sea surface temperatures at the Last Glacial Maximum, *Geophys. Res. Lett.*, *27*(1), 105–108, 2000.

Mahowald, N., K. Kohfeld, M. Hansson, Y. Balkanski, S. P. Harrison, I. C. Prentice, M. Schulz, and H. Rodhe, Dust sources and deposition during the Last Glacial Maximum and current climate: A comparison of model results with paleodata from ice cores and marine sediments, *J. Geophys. Res.*, *104*(D13), 15,895–15,916, 1999.

Marticorena, B., and G. Bergametti, Modeling the atmospheric dust cycle: Design of a soil-derived dust emission scheme, *J. Geophys. Res.*, *100*(D8), 16,415–16,430, 1995.

Martin, J. H., Iron still comes from above, *Nature*, *353*, 123, 1991.

Mayewski, P. A., et al., Changes in atmospheric circulation and ocean ice cover over the North Atlantic during the last 41,000 years, *Science*, *263*, 1747–1751, 1994.

Mayewski, P. A., L. D. Meeker, M. S. Twickler, S. Whitlow, Q. Z. Yang, W. B. Lyons, and M. Prentice, Major features and forcing of high-latitude Northern Hemisphere atmospheric circulation using a 110,000-year-long glaciochemical series, *J. Geophys. Res.*, *102*(C12), 26,345–26,366, 1997.

McTainsh, G. H., Quaternary aeolian dust processes and sediments in the Australian region, *Quat. Sci. Rev.*, *8*, 235–253, 1989.

Middleton, N. J., and A. S. Goudie, Saharan dust: Sources and trajectories, *Trans. Inst. Brit. Geogr.*, *26*(2), 165–181, 2001.

Middleton, N. J., A. S. Goudie, and G. L. Wells, The frequency and source areas of dust storms, in *Aeolian Geomorphology*, edited by W. G. Wickling, pp. 237–260, Inst. of Brit. Geogr., London, 1986.

Mix, A. C., A. E. Morey, N. G. Pisias, and S. W. Hostetler, Foraminiferal faunal estimates of paleotemperature: Circumventing the no-analog problem yields cool ice age tropics, *Paleoceanography*, *14*(3), 350–359, 1999.

Monsi, M., and T. Saeki, Über den Lichtfaktor in den Pflanzengesellschaften und seine Bedeutung für die Stoffproduktion, *Jpn. J. Bot.*, *14*, 22–52, 1953.

Ohkouchi, N., K. Kawamura, T. Nakamura, and A. Taira, Small changes in the sea-surface temperature during the last 20,000 Years: Molecular evidence from the western tropical Pacific, *Geophys. Res. Lett.*, *21*(20), 2207–2210, 1994.

Orgill, M. M., and G. A. Sehmel, Frequency and diurnal variation of dust storms in contiguous U.S.A., *Atmos. Environ.*, *10*(10), 813–825, 1976.

Parungo, F., et al., Asian dust storms and their effects on radiation and climate, *Tech. Rep. STC2906*, Natl. Oceanic and Atmos. Admin., Silver Spring, Md., 1995.

Peltier, W. R., Ice age paleotopography, *Science*, *265*, 195–201, 1994.

Pinot, S., G. Ramstein, S. P. Harrison, I. C. Prentice, J. Guiot, M. Stute, and S. Joussaume, Tropical paleoclimates at the Last Glacial Maximum: Comparison of Paleoclimate Modeling Intercomparison Project (PMIP) simulations and paleodata, *Clim. Dyn.*, *15*(11), 857–874, 1999a.

Pinot, S., G. Ramstein, I. Marsiat, A. de Vernal, O. Peyron, J. C. Duplessy, and M. Weinelt, Sensitivity of the European LGM climate to North Atlantic sea-surface temperature, *Geophys. Res. Lett.*, *26*(13), 1893–1896, 1999b.

Prospero, J. M., *The Atmospheric Transport of Particles to the Ocean*, John Wiley, New York, 1996.

Prospero, J. M., and R. T. Nees, Impact of the North African drought and El Niño on mineral dust in the Barbados trade winds, *Nature*, *320*, 735–738, 1986.

Pye, K., *Aeolian Dust and Dust Deposits*, 334 pp., Academic, San Diego, Calif., 1987.

Pye, K., and L.-P. Zhou, Late Pleistocene and Holocene aeolian dust deposition in north China and the northwest Pacific Ocean, *Palaeogeogr. Palaeoclimatol. Palaeoecol.*, *73*, 11–23, 1989.

Ram, M., and G. Koenig, Continuous dust concentration profile of pre-Holocene ice from the Greenland Ice Sheet Project 2 ice core: Dust stadials, interstadials, and the Eemian, *J. Geophys. Res.*, *102*(C12), 26,641–26,648, 1997.

Ram, M., M. Stolz, and G. Koenig, Eleven year cycle of dust concentration variability observed in the dust profile of the GISP2 ice core from Central Greenland: Possible solar cycle connection, *Geophys. Res. Lett.*, *24*(19), 2359–2362, 1997.

Rochon, A., A. de Vernal, H. P. Sejrup, and H. Haflidason, Palynological evidence of climatic and oceanographic changes in the North Sea during the last deglaciation, *Quat. Res.*, *49*(2), 197–207, 1998.

Roeckner, E., K. Arpe, L. Bengtsson, M. Christoph, M. Claussen, L. Dümenil, M. Esch, M. Giorgetta, U. Schlese, and U. Schulzweida, The atmospheric general circulation model ECHAM4: Model description and simulation of present-day climate, *Tech. Rep. 218*, Max-Planck-Inst. for Meteorol., Hamburg, Germany, 1996.

Roelandt, C., Coupled simulation of potential natural vegetation, terrestrial carbon balance and physical land-surface properties with the ALBIOC model, *Ecol. Model.*, *143*(3), 191–214, 2001.

Rosell-Melé, A., M. Weinelt, M. Sarnthein, N. Koç, and E. Jansen, Variability of the Arctic front during the last climatic cycle: Application of a novel molecular proxy, *Terra Nova*, *10*(2), 86–89, 1998.

Sokolik, I. N., and O. B. Toon, Direct radiative forcing by anthropogenic airborne mineral aerosols, *Nature*, *381*, 681–683, 1996.

Sonzogni, C., E. Bard, and F. Rostek, Tropical sea-surface temperatures during the last glacial period: A view based on alkenones in Indian Ocean sediments, *Quat. Sci. Rev.*, *17*(12), 1185–1201, 1998.

Steffensen, J. P., Analysis of the seasonal variation in dust, Cl^-, NO_3^- and SO_4^{2-} in two central Greenland firn cores, *Ann. Glaciol.*, *10*, 171–177, 1988.

Swap, R. M., M. Garstang, S. Greco, R. Talbot, and P. Kallberg, Saharan dust in the Amazon basin, *Tellus, Ser. B*, *44*, 133–149, 1992.

Taylor, K. C., C. U. Hammer, R. B. Alley, H. B. Clausen, D. Dahl-Jensen, A. J. Gow, N. S. Gundestrup, J. Kipfstuhl, J. C. Moore, and E. D. Waddington, Electrical conductivity measurements from the GISP2 and GRIP Greenland ice cores, *Nature*, *366*, 549–552, 1993.

Tegen, I., and I. Fung, Contribution to the atmospheric mineral aerosol load from land surface modification, *J. Geophys. Res.*, *100*(D9), 18,707–18,726, 1995.

Tegen, I., S. P. Harrison, K. Kohfeld, I. C. Prentice, M. Coe, and M. Heimann, The impact of vegetation and preferential source areas on global dust aerosols: Results from a model study, *J. Geophys. Res.*, *107*, 4576, doi:10.1029/2001JD000963, 2002.

Unnerstad, L., and M. Hansson, Simulated airborne particle size distributions over Greenland during Last Glacial Maximum, *Geophys. Res. Lett.*, *28*(2), 287–290, 2001.

Weinelt, M., M. Sarntheim, U. Pflaumann, H. Schulz, S. Jung, and H. Erlenkeuser, Ice-free Nordic Seas during the Last Glacial Maximum? Potential sites of deepwater formation, *Paleoclimates*, *1*, 283–309, 1996.

Werner, M., U. Mikolajewicz, M. Heimann, and G. Hoffmann, Borehole versus isotope temperatures on Greenland: Seasonality does matter, *Geophys. Res. Lett.*, *27*(5), 723–726, 2000.

Werner, M., M. Heimann, and G. Hoffmann, Isotopic composition and origin of polar precipitation in present and glacial climate simulations, *Tellus, Ser. B*, *53*, 53–71, 2001.

Wolff, T., S. Mulitza, H. Arz, J. Patzold, and G. Wefer, Oxygen isotopes versus CLIMAP (18 ka) temperatures—A comparison from the tropical Atlantic, *Geology*, *26*(8), 675–678, 1998.

Wurzler, S., T. G. Reisin, and Z. Levin, Modification of mineral dust particles by cloud processing and subsequent effects on drop size distributions, *J. Geophys. Res.*, *105*(D4), 4501–4512, 2000.

Yu, G., et al., Palaeovegetation of China: A pollen data-based synthesis for the mid-Holocene and Last Glacial Maximum, *J. Biogeogr.*, *27*(3), 635–664, 2000.

Zhang, Y., and G. R. Carmichael, The role of mineral aerosol in tropospheric chemistry in East Asia—A model study, *J. Appl. Meteorol.*, *38*(3), 353–366, 1999.

Zhao, M., N. A. S. Beveridge, N. J. Shackleton, M. Sarnthein, and G. Eglinton, Molecular stratigraphy of cores off northwest Africa: Sea surface temperature history over the last 80 ka, *Paleoceanography*, *10*(3), 661–675, 1995.

Zobler, L., A world soil file for global climate modeling, *NASA Tech. Rep. TM-87802*, 32 pp., 1986.

Zolitschka, B., A. Brauer, J. F. W. Negendank, H. Stockhausen, and A. Lang, Annually dated late Weichselian continental paleoclimate record from the Eifel, Germany, *Geology*, *28*(9), 783–786, 2000.

Y. Balkanski, Laboratoire des Sciences du Climat et de l'Environnement, U.M.R. CEA-CNRS, F-91191 Gif-sur-Yvette Cedex, France. (balkansk@lsce.saclay.cea.fr)

S. P. Harrison, K. E. Kohfeld, I. C. Prentice, I. Tegen, and M. Werner, Max-Planck-Institute for Biogeochemistry, Postbox 100164, D-07701 Jena, Germany. (sandy.harrison@bgc-jena.mpg.de; karen.kohfeld@bgc-jena.mpg.de; colin.prentice@bgc-jena.mpg.de; ina.tegen@bgc-jena.mpg.de; martin.werner@bgc-jena.mpg.de)

H. Rodhe, Department of Meteorology, Stockholm University, S-10691 Stockholm, Sweden. (rodhe@misu.su.se)

C. Roelandt, Department of Geography, Université catholique de Louvain, Place Louis Pasteur 3, B-1348 Louvain-la-Neuve, Belgium. (roelandt@geog.ucl.ac.be)